Species-Specific Differences in the Medial Prefrontal Projections to the Pons Between Rat and Rabbit

Maria V. Moya,[1] Jennifer J. Siegel,[1]* Eedann D. McCord,[1] Brian E. Kalmbach,[1] Nikolai Dembrow,[1] Daniel Johnston,[1,2] and Raymond A. Chitwood[1]

[1]Center for Learning & Memory, University of Texas at Austin, Austin, Texas 78712
[2]Department of Neuroscience, University of Texas at Austin, Austin, Texas 78712

ABSTRACT

The medial prefrontal cortex (mPFC) of both rats and rabbits has been shown to support trace eyeblink conditioning, presumably by providing an input to the cerebellum via the pons that bridges the temporal gap between conditioning stimuli. The pons of rats and rabbits, however, shows divergence in gross anatomical organization, leaving open the question of whether the topography of prefrontal inputs to the pons is similar in rats and rabbits. To investigate this question, we injected anterograde tracer into the mPFC of rats and rabbits to visualize and map in 3D the distribution of labeled terminals in the pons. Effective mPFC injections showed labeled axons in the ipsilateral descending pyramidal tract in both species. In rats, discrete clusters of densely labeled terminals were observed primarily in the rostromedial pons. Clusters of labeled terminals were also observed contralateral to mPFC injection sites in rats, appearing as a less dense "mirror-image" of ipsilateral labeling. In rabbits, mPFC labeled corticopontine terminals were absent in the rostral pons, and instead were restricted to the intermediate pons. The densest terminal fields were typically observed in association with the ipsilateral pyramidal tract as it descended ventromedially through the rabbit pons. No contralateral terminal labeling was observed for any injections made in the rabbit mPFC. The results suggest the possibility that mPFC inputs to the pons may be integrated with different sources of cortical inputs between rats and rabbits. The resulting implications for mPFC or pons manipulations for studies of trace eyeblink in each species are discussed. J. Comp. Neurol. 522:3052–3074, 2014.

INDEXING TERMS: PFC; corticopontine; anterograde tracer; pontine nuclei; corticocerebellar

An understanding of how the brain supports learning and memory requires knowledge of the specific connectivity between participating brain regions and the motor systems that mediate and express learning. Trace eyeblink conditioning is an example of associative learning that requires an interaction between forebrain regions and the cerebellum, via the pontine nuclei (Clark et al., 2002; Kalmbach et al., 2009, 2010; Weiss and Disterhoft, 2011; Siegel et al., 2012). After many pairings of a conditioned stimulus (CS, e.g., a tone) with an unconditioned stimulus (US, e.g., a puff of air to the eye initiating a reflexive eyeblink closure), animals learn that the CS predicts the US and close the eyeblink in anticipation of the US. When the CS and US are separated by a stimulus-free interval ("trace" eyeblink conditioning) the cerebellum relies on additional input from the forebrain to bridge the temporal gap between stimuli to learn and express conditioned responses. Rabbits and rats are both able to learn this task, with lesion studies indicating that both the medial prefrontal cortex (mPFC) and cerebellum are necessary for the expression of conditioned responses (Kronforst-Collins and Disterhoft, 1998; Takehara et al., 2003; Weible et al., 2003; Powell et al., 2005; Kalmbach, 2008), and single-unit studies in the mPFC revealing neural activity capable of bridging the trace interval (Takehara-Nishiuchi and McNaughton, 2008; Siegel et al., 2012). However, there are some apparent differences in learning between the two

The first two authors contributed equally to this work.

Grant sponsor: National Institutes of Health (NIH); Grant numbers: MH094839 (to D.J. and M.D.M.), NS084473 (to D.J.), MH46904 and MH74006 (to M.D.M.); Grant sponsor: the McKnight Foundation.

*CORRESPONDENCE TO: Jennifer J. Siegel, Center for Learning & Memory, University of Texas at Austin, 1 University Station Stop C7000, Austin, TX 78712-0805. E-mail: jenni@mail.clm.utexas.edu

Received September 19, 2013; Revised January 18, 2014;
Accepted February 18, 2014.
DOI 10.1002/cne.23566
Published online February 22, 2014 in Wiley Online Library (wileyonlinelibrary.com)

species. For example, most rats are unable to meet a standard learning criterion (e.g., 60% response rate) with a trace interval of 500 ms (Weiss et al., 1999; Takehara et al., 2003; Takehara-Nishiuchi et al., 2006; Nokia et al., 2012), while rabbits show robust learning with trace intervals of 500 ms (Thompson et al., 1996; Kalmbach et al., 2009, 2010; Siegel et al., 2012). The neural basis for such differences is currently unknown, but addressing such questions begins with an understanding of the species-specific differences in prefrontal-pons-cerebellar projection patterns.

Previous work in rabbits has provided an initial mapping of the prefrontopontine projections that is the anatomical basis for the expression of learning in the trace eyeblink conditioning circuit (Buchanan et al., 1994; Weible et al., 2007; Siegel et al., 2012). Our goal was to extend the previous work in rabbits and to provide a comparative mapping for the trace eyeblink conditioning circuit in rats. To this end, we made discrete injections of fluorescent dextran amines in regions of the mPFC of rats and rabbits which previous work showed was necessary for trace conditioning (compare Fig. 1 to Takehara et al., 2003; Kalmbach et al., 2009), and visualized labeled terminals in the pons. The anterograde tracer revealed species-specific differences in the rostrocaudal extent of prefrontal terminals in the ipsilateral pons, as well as the presence of projections to the contralateral pons in rat that was distinctly absent in rabbit. The results suggest that prefrontal inputs to the pons may be integrated with different kinds of cortical inputs between rats and rabbits, and that the rat prefrontal cortex may also support tasks that require bilateral coordination of the cerebellum.

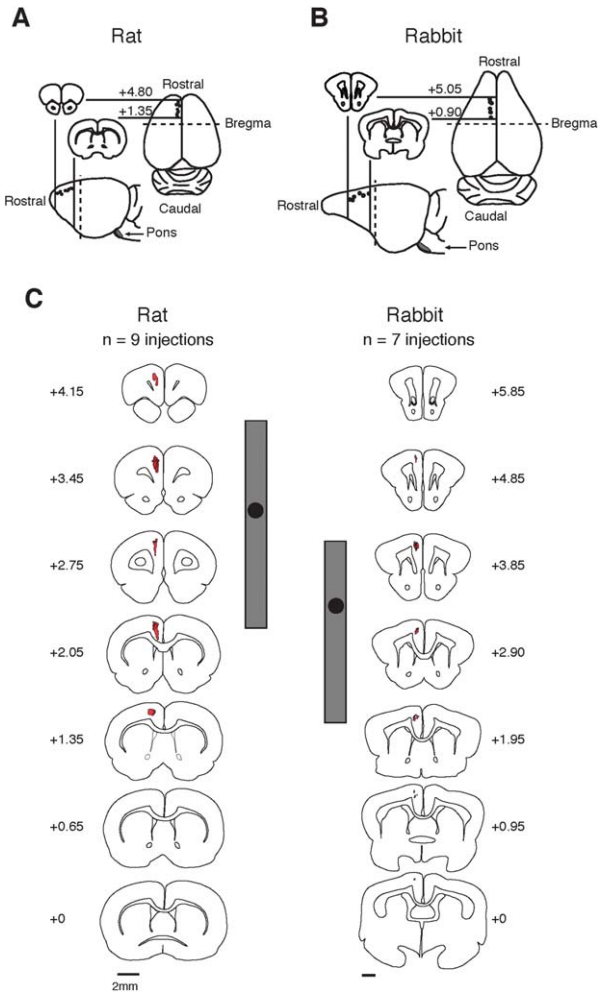

Figure 1. Schematics showing anterograde tracer injection sites within the mPFC of rats and rabbits. **A:** Representations of the rat brain showing the locations of prefrontal injection sites ($n = 9$ injections in seven animals, round markers) from dorsal (top right) and lateral (bottom left) perspectives. Coronal representations (top left) indicate structure at the most rostral and caudal injection sites (numbers indicate stereotaxic rostrocaudal coordinates relative to Bregma). Location of the pons relative to the injection sites is indicated in the lateral perspective (gray shaded region). **B:** Representations of the rabbit brain showing the locations of prefrontal injection sites ($n = 7$ injections in five animals), as described for rats in A. **C:** Example coronal sections from along the rostrocaudal axis of mPFC (numbers indicate stereotaxic coordinates relative to Bregma). Cumulative extent of layer V tissue containing labeled somata across all cases for rat and rabbit is shown in red. Boxplots (center) show the COM of labeled prefrontal tissue (black markers) and IQR (gray box) for rats and rabbits. Note that 75% of labeled prefrontal layer V tissue overlaps in the rostrocaudal axis, and was injected in anatomically similar prefrontal regions.

MATERIALS AND METHODS

Infusion of anterograde tracer

All procedures were approved by the University of Texas at Austin Institutional Animal Care and Use Committee and were in accordance with the National Institutes of Health guidelines. The mPFC of rats and rabbits were injected with a 10% solution of 10,000 MW dextran amines containing a fixable lysine residue and conjugated to Alexa 488 or 594 (D22910 and D22913, Invitrogen Molecular Probes, Grand Island, NY), dissolved in artificial cerebrospinal fluid (in mM: 119.0 NaCl, 2.5 KCl, 1.2 NaH_2PO_4, 26.0 $NaHCO_3$, 2.0 $CaCl_2$, 2.0 $MgCl_2$, 10.0 dextrose, 10.0 HEPES; pH adjusted to between 7.35 and 7.4 and passed through a 2-μm filter to sterilize). Each animal received at most two injections in the mPFC: one at a caudal mPFC site, and in most cases a second ipsilateral injection using a different color fluorophore at a more rostral site. A dedicated Hamilton (Reno, NV) syringe was paired with a given fluorophore across surgeries to avoid any possibility of contamination between injection sites.

Rats

Male Sprague–Dawley rats ($n = 8$, 250–400 g; Charles River Laboratories, Wilmington, MA) were anesthetized with isofluorane (4% induction followed by 1–3% maintenance). Each animal was placed in a stereotaxic apparatus and the skull leveled based on the dorsal-ventral coordinates of Bregma and Lambda (Paxinos and Watson, 2007). Craniotomies were made over the target regions of mPFC (between 1 and 5 mm anterior to Bregma, 1 mm lateral to the midline; Figs. 1–3).{FIG1–3} After the dura was retracted, a 1 μL Hamilton syringe (model 7001KH, Fisher-Scientific, Pittsburgh, PA) was filled with 0.25 μL of dextran tracer, and the syringe tip lowered 1.5 mm below the surface of the brain and allowed to settle for 10 minutes before beginning manual pressure injection. Each animal received two ipsilateral injections, one at a rostral location (3.0–5.0 mm rostral to Bregma) and a second using a different color fluorophore at a more caudal coordinate (1.0–2.5 mm rostral to Bregma). Tracer was pressure injected over 5 minutes (0.05 μL/min). The syringe was left in place for a minimum of 10 minutes after injection to allow for diffusion and then withdrawn from the brain. After injections were complete the craniotomies were filled with Kwiksil (World Precision Instruments, Sarasota, FL) and the skin of the animal sutured. Rats survived 5–7 days before sacrifice to allow the anterograde tracer to be transported down the axons and fill terminals in the pons.

Rabbits

New Zealand albino male rabbits ($n = 6$, 3–4 kg; Myrtle's Rabbitry, Thompsons Station, TN) were initially anesthetized with 45 mg/kg ketamine mixed with 1.5 mg/kg acepromazine and placed in a stereotaxic apparatus with Lambda 1.5 mm below Bregma (McBride and Klemm, 1968). Anesthesia was maintained with 1–3% isoflurane throughout surgery. A craniotomy was made over the target region(s) of mPFC (between 1 and 5 mm rostral to Bregma, 1 mm lateral to midline; Figs. 1–3). After the dura was retracted, a 1-μL Hamilton syringe was filled with 1 μL of tracer and the syringe tip lowered 1.5 to 2.0 mm below the surface of the brain and allowed to settle for 10 minutes before manual infusion of tracer. Anterograde tracer was pressure injected over a 20-minute period (0.05 μL/min), after which the syringe was left in place for 10 minutes before being withdrawn. Each rabbit received an injection at a caudal mPFC location, and three of the rabbits received a second injection using a different fluorophore at a more rostral location. Craniotomies were filled with Kwiksil and the skin of the animal sutured. Rabbits survived for 7–9 days postsurgery.

Tissue collection and processing

Animals were given lethal injections (rats: ketamine, 160 mg/kg mixed with xylazine, 16 mg/kg, intraperitoneal; rabbits: Euthasol 0.3 mL/kg, intravenous) and perfused intracardially with cold, 0.9% physiological saline or oxygenated modified artificial cerebrospinal fluid (aCSF) (2.5 mM KCl, 1.25 mM NaH_2PO_4, 25 mM $NaHCO_3$, 0.5 mM $CaCl_2$, 7 mM $MgCl_2$, 7 mM dextrose, 205.5, mM sucrose, 1.3 mM ascorbic acid, and 3.7 mM pyruvate), followed by 4% paraformaldehyde in 0.02 or 0.1 M phosphate buffer (pH 7.4). Brains were postfixed for at least 2 days and then transferred in a 30% sucrose solution until equilibrated for cyroprotection. Tissue was sectioned using a sliding microtome (Leica Microsystems, Buffalo Grove, IL) equipped with temperature controlled freezing stage (Physitemp, Clifton, NJ). Coronal sections of the mPFC (50–100 μm) and the pons (50 μm) were transferred to 0.9% physiological saline and mounted on Microfrost Plus slides (Fisher Scientific). Mounted sections were protected from light and dust, and air-dried overnight. Prior to coverslipping, sections were washed in 50% EtOH (1 minute), followed by 100% EtOH (1 minute), and then cleared in xylenes for 10 minutes and coverslipped with DPX mounting medium (Electron Microscopy Services, Hatfield, PA).

Image acquisition and processing

Images of mPFC and pons sections were acquired using a Zeiss Axio Imager Z2 microscope running AxioVision software (v. 4.8.2; Carl Zeiss, Thornwood, NY). Multichannel images were acquired and included up to three independent reflected wavelength bands (blue, green, and red) and one transmitted channel using differential interference contrast. The fluorescent channels included: one optimized for viewing the nuclear stain 4′,6-diamidino-2-phenylindole dilactate (DAPI) and used here to visualize autofluorescence of gross anatomical structure (blue); another for viewing the fluorophore Alexa-488 (green); and a third for viewing the fluorophore Alexa-594 (red). In the case of conventional fluorescence, standard Zeiss filter sets (set 49: ex G 365, dc 395, em 445/50; set 38: ex 470/40, dc 495, em 525/50; set 71: ex 592/24, dc 615, em 675/100; for blue, green, and red, respectively) were used to separate the excitation/emission wavelengths. Little or no crosstalk between channels was observed (e.g., Fig. 4A–C). Images were acquired as multichannel mosaics in 12- or 16-bit grayscale format. Following alignment of tiled images and assembly into a single continuous image using the AxioVision software, individual channels were exported as unmodified 8- or 12-bit TIF files.

A subset of images were reacquired using a Leica SP5-RS 2-photon laser-scanning microscope running the

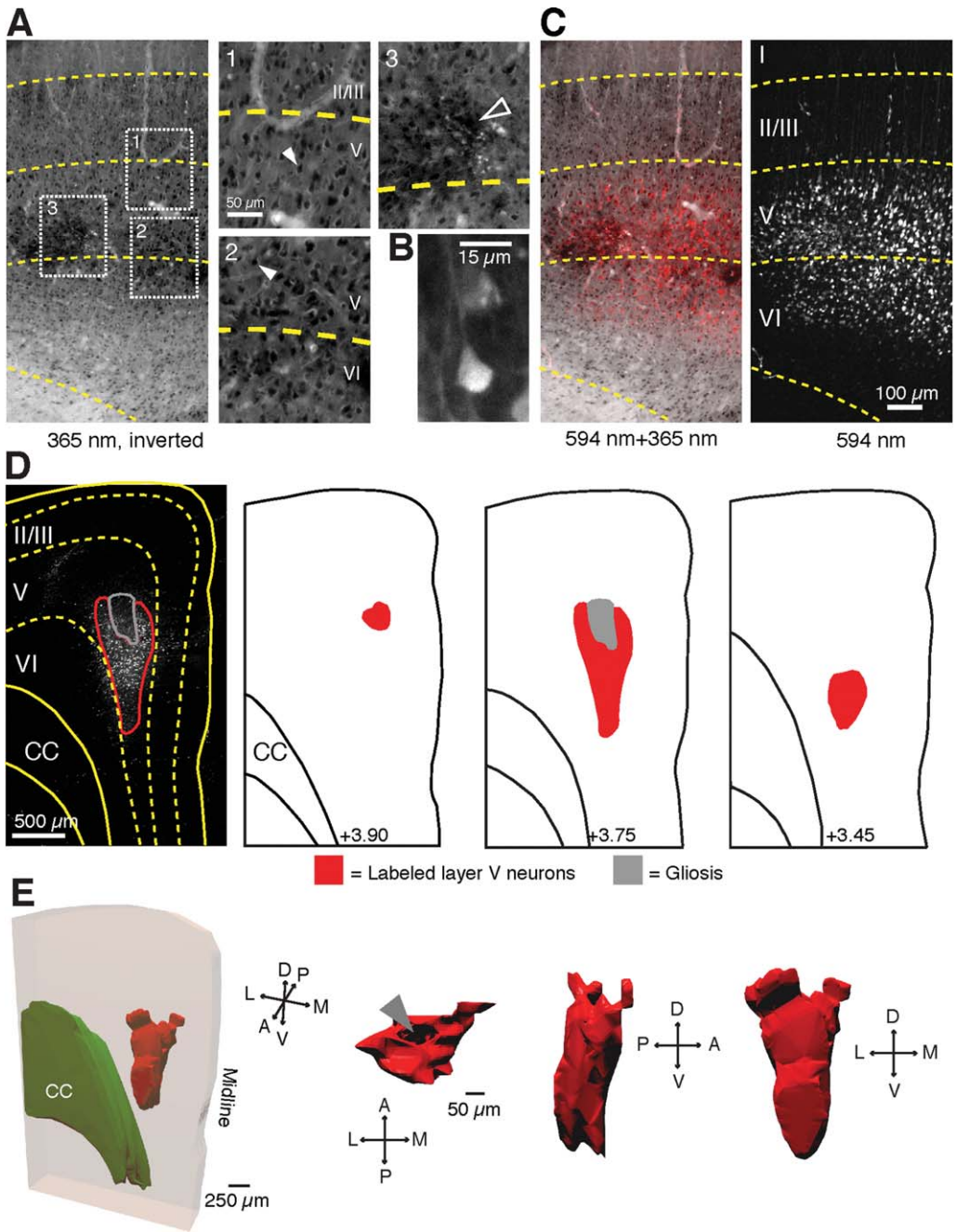

Figure 2. Identification of labeled layer V somata at prefrontal injection sites. **A,B:** Inverted autofluorescent (blue channel) images showing delineation of neocortical cell layers in medial prefrontal cortex based on cell morphology (dashed yellow lines). Closed arrows show identified pyramidal cells (one is shown at higher magnification in B, autofluorescence not inverted here), open arrow shows example of gliotic tissue. Boxes 1–3 show the corresponding subregions at higher magnification. **C:** Fluorescent image (right) overlaid over inverted autofluorescent image (left) used to identify neocortical layers. **D:** Fluorescent image with outlines of cortical surface and corpus callosum (solid yellow lines) and neocortical cell layers (dashed lines), and outline of labeled layer V tissue (red line) and gliosis (gray line) for a single coronal section. Line drawings show identified labeled tissue (red) and regions of gliosis (gray) at more anterior (left) and posterior (right) coronal sections. **E:** Three-dimensional rendering of all prefrontal sections from this case showing the overall 3D structure of labeled layer V tissue (far left), also shown from three additional rotated perspectives as indicated by directional compasses (left to right). A, anterior; P, posterior; D, dorsal; V, ventral; M, medial; L, lateral. Filled gray arrow indicates region of gliotic tissue.

Leica Application Suite Advanced Fluorescence software and using Dodt contrast enhancement. When 2-photon excitation was used, the excitation wavelength was set to 840 nm and the reflected green and red signals separated using standard filters (dichroic: DXCR 565; green bandpass: HQ 525/50; red bandpass: HQ

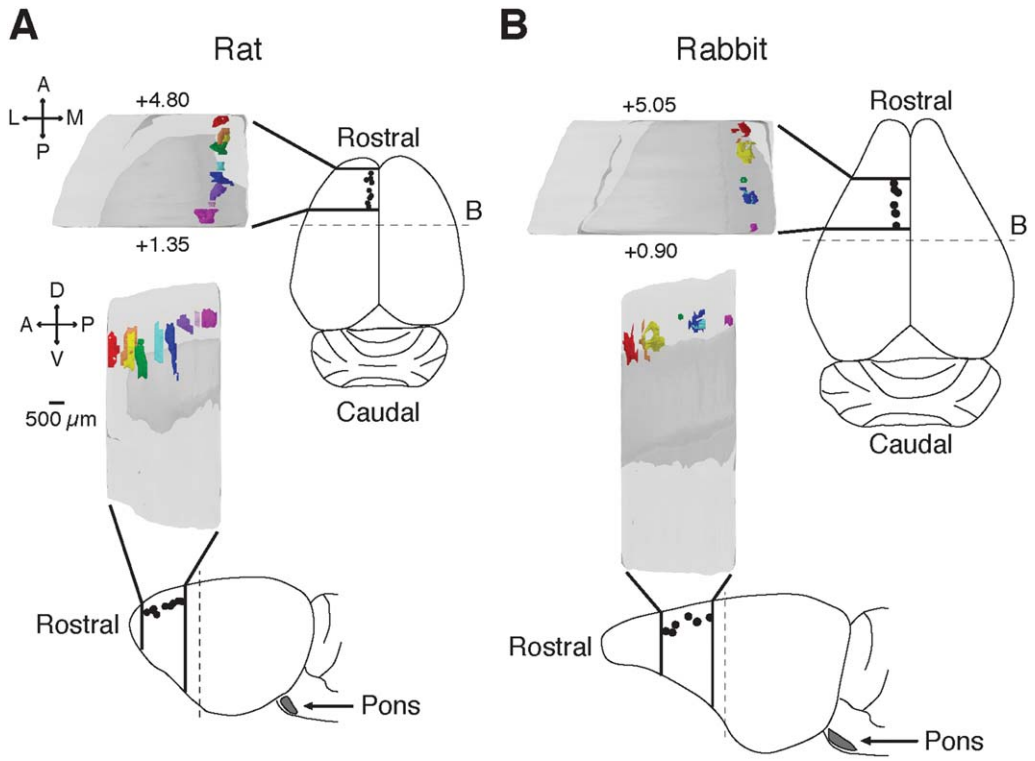

Figure 3. Three-dimensional rendering of all medial prefrontal injection sites in rat (**A**) and rabbit (**B**). Different colors represent different individual cases for each species. Numbers represent anterior-posterior stereotaxic coordinates relative to Bregma (B), directional compasses are as given in Figure 2. Note that a similar relative span of the medial prefrontal cortex was sampled in the two species.

645/100) in an external, non-descanned detector. In rare instances where the fluorescent signal was weak, both the reflected and transmitted fluorescent emission was collected to increase the signal-to-noise ratio.

Images from both conventional and two-photon techniques were processed using ImageJ (NIH, http://rsbweb.nih.gov/ij) or FIJI (Schindelin et al., 2012). Unprocessed image stacks were imported using Bio-Formats import utilities (Open Microscopy Environment, http://openmicroscopy.org; Linkert et al., 2010). Images were adjusted to maximize the distribution of pixel values in an effort to increase contrast and minimize background autofluorescence in the green and red channels. Because the smallest processes were sometimes difficult to resolve against the background tissue autofluorescence, the autofluorescence of a second channel was subtracted from the original to enhance the signal-to-noise ratio (Fig. 4A–C). Care was taken to ensure the background autofluorescence was equivalent in each channel—the mean fluorescence was measured in an area devoid of labeled tissue and the images adjusted to normalize the level of background across green and red channels. Adjusted images were always compared to their respective unaltered source files to ensure the process eliminated the appropriate amount of autofluorescence from the original image. This method worked equally well for subtracting autofluorescence from either the green or red channel images. Because the resulting image lacked information regarding gross morphology, the autofluorescence from the blue channel was optimized and inverted for the sole purpose of visualizing the overall anatomical structure of a given section.

Localization of mPFC injection sites

Fluorescent images of all mPFC sections were initially acquired at 2.5× magnification to view the general infusion location, and again at 10× to determine the extent of labeled neurons across mPFC subregions and cortical layers (Fig. 2A–D). An anterior-posterior stereotaxic coordinate relative to Bregma was assigned to each section by first designating the section containing the genu of the corpus callosum as a reference point according to the atlases of Paxinos and Watson (2007; rats, +2.30 mm from Bregma; Fig. 3 left panel) or McBride and Klemm (1968; rabbits, +3.25 mm from Bregma; Fig. 3 right panel) and assigning an anterior-posterior coordinate to subsequent sections rostral and caudal to that point based on section thickness.

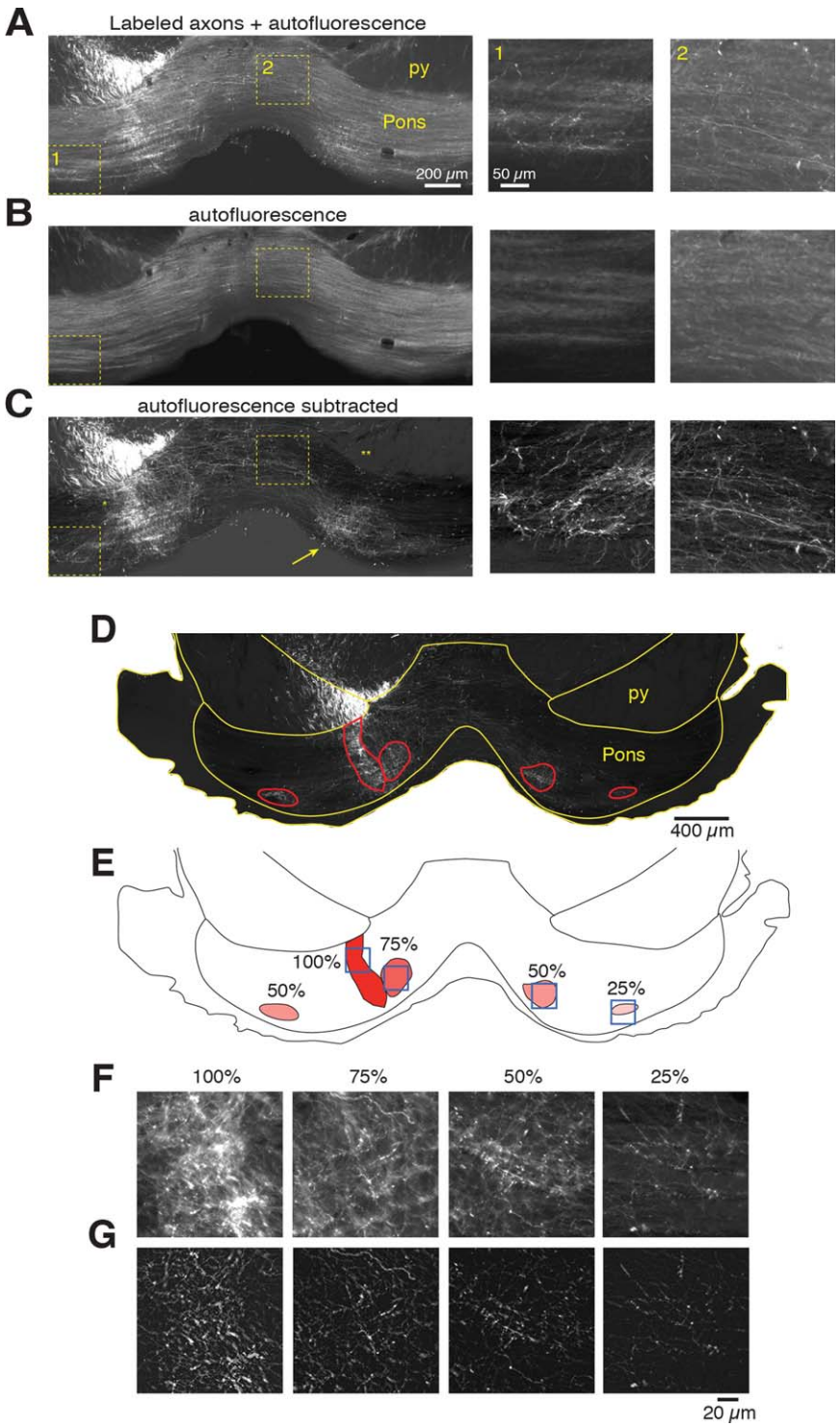

Figure 4. Identification of clusters of putative prefrontal axon terminals and relative terminal density assignments. **A–C:** Example of autofluorescence-subtracted processing of pons images. To ensure that even lightly or sparsely labeled terminal clusters would be detected (example regions of light, box 1, and sparse, box 2, are given in A), relative background autofluorescence was normalized between the red and green channels, and then the normalized background fluorescence (determined from areas where no labeling was ever observed) was subtracted from the channel of interest resulting in readily identifiable axons and terminals (C, right). Note that there was no apparent cross-talk in fluorescent signals between the red and green channels (B). **D:** Autofluorescence-subtracted pons image with outlines of the pontine gray (Pons) and pyramidal tract (py) in yellow, and identified terminal clusters outlined in red. **E:** Cluster outlines were filled and opacity adjusted to reflect the relative density of punctate terminals observed (ranging from 100% being the most dense observed in that animal to 25%). **F,G:** Examples of the density assignments before (F) and after (G) autofluorescence-subtraction, from example regions outlined in D,E.

Localization of pons labeling

Pons tissue was imaged at 10× magnification. The rostral-caudal coordinates of pons sections were determined by assigning an anterior-posterior coordinate of the most rostral section of the pons based on gross anatomical features according to the atlases of Paxinos and Watson (2007) or McBride and Klemm (1968) and assigning an anterior-posterior coordinate to subsequent sections caudal to that point based on section thickness.

Analysis

Inclusion of data for analysis

Eight rats each received two injections targeted to separate locations along the rostral-caudal axis of the mPFC. Of the 15 mPFC injections in the rat (one injection fell outside of the mPFC and was excluded), nine injections resulted in clearly labeled axons in the descending pyramidal tract ipsilateral to the injection site (Fig. 4 shows an example of such labeling), indicating effective uptake and transport of the dextran by mPFC layer V neurons. These nine cases were included for further analysis (Figs. 1A,C, 3A). The six remaining cases were either devoid of labeled axons in the pyramidal tract ($n = 5$ cases) or showed very sparsely labeled axons ($n = 1$ case) relative to the extent of labeling typically observed. Double-labeled axons in the pyramidal tract or pons were not observed, suggesting that there was no diffusion of tracer across injection sites. Labeled axons were never observed in the contralateral pyramidal tract (e.g., Fig. 4).

Six rabbits received anterograde tracer injections in the mPFC (four rabbits received two injections, as described for rats, and two rabbits received a single more caudal injection). The data from the two rabbits with single caudal injections have been previously reported (Siegel et al., 2012). In 7 of 10 experiments labeled axons were observed in the ipsilateral descending pyramidal tract and were included for analysis (locations shown in Figs. 1B, 3B). The remaining three cases resulted in minimal labeling of layer labeling of axons in the pyramidal tract and no terminal labeling observed in the pons. Similar to rats, labeled axons in the pyramidal tract contralateral to the injection site were never observed, and no double-labeling was present.

The corpus callosum is located immediately adjacent to the mPFC in rats and rabbits (e.g., Fig. 2E, CC in left panel). This dense bundle of axons was largely undisturbed by the insertion of the syringe during dextran injections in all cases. Although in some cases tracer did diffuse to the corpus callosum, no evidence of uptake directly by corpus callosum axons of passage was observed (similar to previous observations; Glover et al., 1986; Schmued et al., 1990). Labeled axons were observed to enter the corpus callosum, typically from the shoulder cortex area of mPFC, and were also observed exiting the corpus callosum at the same location in the contralateral hemisphere. No labeling of soma in the contralateral mPFC was ever observed. The contralateral projection between subregions of mPFC has been previously described and was not analyzed here (Sesack et al., 1989; Buchanan et al., 1994; Weible et al., 2007)

Restriction of mPFC injection sites to tissue containing labeled layer V neurons

It was previously shown that mPFC projections to the pons originate exclusively from layer V neurons (Legg et al., 1989). We therefore restricted our injection site measurements to dextran-labeled layer V cells.

Images of mPFC sections were imported as TIF files into the serial-section reconstruction software Reconstruct (http://synapses.clm.utexas.edu; Fiala, 2005) and aligned using the midline and the dorsal surfaces of each section as anchors. The boundaries of layer V in all mPFC sections were determined by comparing neuron somatic morphology readily discerned in the inverted blue-channel image (e.g., Fig. 2A,B). The identification of cortical layer boundaries based on differences in neural morphology allowed for the inclusion of layer V labeled tissue even if displaced by mechanical insertion of the injection syringe. The "Point-by-Point Tracing Tool" within Reconstruct was used to outline regions of layer V tissue containing dextran labeled neurons (e.g., Fig. 2D), which also gave the surface area and 2D centroid (used to calculate the center-of-mass of the labeled tissue; see below). We did not include layer V tissue showing evidence of gliosis, often associated with mechanical placement of the syringe during the injection. In regions of gliosis, the blue-channel autofluorescence image revealed an abundance of small cell bodies that did not show neuronal morphology (e.g., Fig. 2A, open arrow), and were easily identified. The restriction of labeled tissue to layer V and the exclusion of regions of gliosis resulted in irregularly shaped masses of mPFC labeled layer V cells (Fig. 2D,E). The volumes of labeled layer V tissue outlined in all sections associated with a given injection site (given by the surface area of the defined boundary times slice thickness) were used to create a 3D representation of each Alexa-dextran injection (e.g., Figs. 2E, 3). It should be noted the volume of labeled tissue would have been underestimated if any removal of dextran from the soma of neurons at the injection site occurred over time.

Identification of the center of mass of mPFC injection sites

The medial-lateral, dorsal-ventral, and rostral-caudal coordinates of the center of mass (COM) of injection sites were calculated independently using the x or y coordinates from the 2D centroids calculated for each mPFC section (described above), or the z coordinates given by the anterior-posterior stereotaxic coordinate of the mPFC sections, using the following formula:

$$COM_{x,\,y\ or\ z} = \frac{\sum_{i=1}^{n} r_{a_i} \times SA_i}{SA_T}$$

where **COM** is the x, y, or z coordinate of the 3D centroid. $\mathbf{SA}_i$ indicates the surface area of layer V within section ***i*** that contained labeled neurons and $\mathbf{r}_a$ is defined by the x, y, or z value for section ***i***. $\mathbf{SA}_T$ is the sum of all labeled layer V surface areas identified in ***n*** sections. The total volume of labeled layer V tissue was also calculated by multiplying $\mathbf{SA}_T$ by section thickness. Note that the formula assumes a uniform density of labeled neurons in calculating the COM of mPFC injection sites. The injection site COM and volume calculations reflect the overall extent of labeled tissue and was insensitive to the density of labeled cells.

The cumulative interquartile range (IQR) of the mass of each reconstructed 3D injection site was calculated to describe the spread of labeling in layer V tissue along the rostral-caudal axis. The quartiles were determined by multiplying the total mass by 0.25 to determine the 25th percentile, and by 0.75 to determine the 75th percentile. The mass from each section was then cumulatively added in rostral-to-caudal order until the 25th and 75th percentiles of the mass were exceeded. The stereotaxic coordinate of the corresponding sections that satisfied the quartiles was used as the IQR, which describes the rostral-caudal range containing 50% of the mass of labeled layer V tissue—the larger the IQR, the greater the spread of labeled tissue across the rostral-caudal axis.

For each species, the injection sites were accumulated across animals to compare total labeled mPFC tissue between rat and rabbit. The rostral-caudal COM was calculated using the same equation as above, with $\mathbf{SA}_i$ given as the sum of surface areas of identified labeled tissue from all injections at given sections from the same stereotaxic coordinate and $\mathbf{SA}_T$ equal to the sum of all surface areas for all injection sites. The same procedure used to calculate the IQRs was applied to the group summed mPFC injections as well.

In addition to calculating the COM, the extent of the injections was examined to determine which mPFC subregions showed labeled layer V tissue. The subregional boundaries of mPFC (medial agranular, AGm; anterior cingulate cortex, AC; prelimbic cortex, PL; infralimbic cortex was not investigated here) were estimated according to differences in laminar morphology (as described by Terreberry, 1987). Labeled layer V tissue that extended beyond the estimated boundary was considered to have labeled that subregion.

Identification of mPFC terminal labeling in the pons and center of mass calculation

After acquiring and processing images of pons tissue, discrete clusters of labeled terminals within each section were identified using ImageJ or FIJI. The boundaries around each discrete cluster of labeled terminals in each pons section were defined using an outline tool, and the area of each identified cluster calculated by converting the number of pixels enclosed with the boundary to area in μm^2. The density of labeled terminals within discrete clusters varied from relatively dense to fairly sparse, even within the same pons section (e.g., Fig. 4E–G). Therefore, density coefficients of 1.0, 0.75, 0.5, or 0.25 were assigned to each cluster, with 1.0 equivalent to the most dense clustering of labeled terminals observed for a given animal, and 0.25 representing relatively sparse density (e.g., Fig. 4E; Jones et al., 2005; Weible et al., 2007). Because light scatter from dense terminal clusters outside the focal plane may have obscured individual presynaptic elements, and to verify that the assigned cluster density was not erroneously influenced by unfocused fluorescence, a subset of sections were examined using 2-photon imaging techniques and validated the assignments given using conventional fluorescent microscopy (compare Fig. 4F to 4G). For illustrative purposes, the assigned density coefficients were represented in figures by the opacity value of the represented cluster boundaries (100, 75, 50, and 25%), where an opacity of 100% indicates a density coefficient of 1.0, and less opaque regions indicate density coefficients proportional to the level of opaqueness (e.g., Fig. 4E). Occasionally, relatively large and highly irregular clusters were observed that appeared to have nonuniform densities across the area, but nevertheless appeared to be a continuous cluster. In these atypical cases the cluster was divided in accordance with density changes into two or three clusters and the appropriate density coefficient assigned.

For each injection site, the COM of pons terminal labeling in the rostral-caudal axis was calculated according to the following equation:

$$COM_z = \frac{\sum_{i=1}^{n} r_i \times SA_i \times \rho_i}{\sum_{i=1}^{n} SA_i \times \rho_i}$$

where, $\mathbf{r}_i$ is the estimated rostral-caudal coordinate of the section in which terminal cluster ***i*** is found, $\mathbf{SA}_i$ is

the surface area of the terminal cluster in the section and ρ_i is its density coefficient. The denominator represents the total mass of the 3D cluster of terminals. The IQR of terminal labeling in the pons was calculated for each injection site using the same procedure as applied to labeled layer V mPFC tissue. To quantify the overall extent of labeling in a way that also accounted for the density of labeling without excluding sparse inputs, we weighted them according to assigned density coefficients (i.e., the area of each cluster was multiplied by its density coefficient). Although a minimum designation of 0.25 was used, sparse clusters tended to be relatively small and thus did not have a substantial impact on the results. Also, similar to the procedure for mPFC injection sites, the terminal clusters observed for all cases for a given species were collapsed to allow for grouped summary comparisons in mPFC corticopontine labeling between rat and rabbit, and the COMs and IQRs calculated as described above.

3D representations

The mPFC and pons were reconstructed from serial images of Nissl-stained coronal sections (50 μm) using custom software (Reconstruct, http://synapses.clm.utexas.edu; Fiala, 2005). The serial sections of a given sample were aligned according to the structural features in consecutive sections. For each section of mPFC, the cortical surface, corpus callosum, and layer V were manually outlined (e.g., Fig. 2C,D). Layer V tissue that contained fluorescent dextran-labeled somata was also manually outlined if present (Fig. 2D). For each section of pons, the pontine gray and pyramidal tracts were manually outlined (e.g., Fig. 4D,E). Clusters of labeled putative axon terminals were also outlined and filled with an arbitrary color that was adjusted in opacity between 25–100% according to the designated cluster density (0.25–1.0, as described above; e.g., Fig. 4D,E). The serial outlines of each sample of mPFC and pons were rendered as "Boissonnat" 3D surfaces (polygonal faces were automatically constructed to make the outline points of consecutive sections contiguous). Rendered 3D images were exported as VRML 2.0 files and imported to Blender (http://www.blender.org) for further processing. In Blender, the surfaces of 3D objects were passed with a "Smoothing Modifier" function (smoothness factor of 1) to remove jagged vertices and surface inconsistencies. The result was a smoothed object that maintained the dimensions of the original, unsmoothed object. Blender was also used to assign case-specific colors to labeled tissue. The appearance of punctate axon terminals in 3D pons reconstructions were assigned arbitrarily by applying a "Particle System" for each outlined cluster that was composed of spheres with a density coefficient consistent with the density assigned to a given cluster. The spheres of particle clusters were also assigned case-specific colors.

RESULTS

The mPFC of rats and rabbits was injected with anterograde tracer to identify the projection pattern of mPFC layer V neurons to the pons for each species. For each injection site, the COM of tissue containing dextran-labeled layer V neurons was calculated to more accurately describe the location of the mPFC injection in a stereotaxic coordinate frame. The area and respective density of labeled terminals resulting from each injection was then determined and the combined results were mapped onto a series of representative PFC and pons sections and a 3D model constructed from these sections.

mPFC injection sites

Rats

The sites of tracer injections in the rat ($n = 9$) were located 0.5–1.5 mm lateral to the midline, and were distributed between +1.35B and +4.8B (mm anterior to Bregma; Fig. 1A). While fluorescent tracer was often observed across multiple layers of mPFC, diffusing both outward from the base of the syringe and along the entire syringe tract, it has been demonstrated that corticopontine projections arise exclusively from neurons in layer V (e.g., Legg et al., 1989). Therefore, the extent and precise location of labeled mPFC corticopontine neurons was restricted to the volume of layer V tissue in which brightly labeled cells were observed (Fig. 2, see Materials and Methods). Regions of obvious gliosis presumably resulting from mechanical damage associated with syringe insertion could be readily identified and excluded from labeled tissue (e.g., Fig. 2A,D). This likely contributed to irregularly shaped layer V injection sites spanning 200–600 μm across the anterior-posterior extent (median anterior-posterior extent of labeling = 500 μm; e.g., Figs. 2D,E, 3A). Six of the nine injections spanned the entire extent of layer V (e.g., Fig. 2C,D). Although the volume of labeled layer V tissue was relatively restricted, a given injection often labeled more than one subregion of mPFC (6/9 cases), based on relative anatomical location according to the atlas of Paxinos and Watson (2007). The most common sampled mPFC subregion was the medial agranular cortex (AGm; also referred to as M2, Fr2, or PCm), labeled in 7/9 cases ranging from +4.8B to +1.35B. The anterior cingulate cortex (AC) was labeled in 6/9 cases but within a more restricted anterior-posterior range than

AGm (+4.3B and +2.4B). The prelimbic subregion (PL) was also labeled in 6/9 cases (only the dorsalmost aspect at the presumed AC border) ranging between +4.8B and +2.3B (to the genu of the corpus callosum and the caudalmost extent of that subregion). The COM of each injection site was calculated and represented as single markers to define the locations of mPFC injection sites along the rostrocaudal axis shown in Figure 1A (see Methods). Figure 1C shows a collapsed representation of mPFC labeled layer V tissue for all nine cases in rat. The mean of the anterior-posterior coordinate of the COM calculated for each injection site (weighted by each injection's layer V volume) was +3.12B, with 50% of injected tracer observed between +3.80B and +2.25B (Fig. 1C, left boxplot).

Rabbits

The sites of anterograde tracer injections in the rabbit ($n = 7$) were located 1.0–2.0 mm lateral to the midline, and were distributed between +5.05B and +0.9B (Figs. 1B, 3B). Similar to that observed for the rats, the fluorescent tracer typically spanned all cell layers of mPFC, diffusing out from the base of the syringe and was observed along the entire syringe tract, labeling cells in superficial as well as deep layers of the mPFC. Using identical procedures as that described for the rats, the extent and precise location of labeled mPFC corticopontine neurons in rabbits was restricted to the volume of layer V tissue in which brightly labeled cells were observed. Again, the exclusion of gliotic tissue often resulted in irregularly shaped layer V injection sites that in the case of the rabbits spanned 300–900 μm across the anterior-posterior extent of the mPFC (Fig. 3B; median of anterior-posterior extent = 600 μm). This increased spread of labeled tissue was likely due to the increased volume of anterograde tracer injected for rabbit (1.0 μL versus 0.25 μL). However, even with the larger injection sites less tissue as a proportion of total mPFC volume appeared labeled in rabbits relative to rats. Similar to rats, labeled layer V neurons from a given injection site in the rabbits often appeared to span more than one presumed mPFC subregion. The most common sampled mPFC subregion in rabbit was the AGm, labeled in 7/7 cases ranging between +5.05B and +0.9B. The AC was labeled in 6/7 cases across the same anterior-posterior range. The dorsal PL was labeled in one case in rabbit, between +5.05B and +4.45B. Figure 1C (right) shows a collapsed representation of mPFC labeled layer V tissue for all seven cases in rabbit. The mean of the COM calculated for each injection site (weighted by each injection's volume) was +3.48B, with 50% of injected tracer observed between +4.17B and +2.17B (Fig. 1C, right boxplot).

Comparison between rats and rabbits

There was substantial overlap of labeled layer V tissue between rats and rabbits on a relative scale (anchored to the genu of the corpus callosum) along the rostrocaudal axis of the mPFC (~75% overlap between the two species; Fig. 1). Overall, the mPFC injection sites between rats are rabbits were similar in terms of relative placement within mPFC (Figs. 1C, 3). The injection sites between the two species differed in that there were fewer rabbit cases with more rostral infusion sites, and in the proportionately larger extent of labeled layer V tissue in rats given that the rabbit brain is ~50% larger than the rat brain, while the average size of rabbit mPFC labeled tissue was only 20% larger. As a result, there was less complete sampling of the rabbit mPFC across the rostrocaudal axis compared to that obtained for the rat.

mPFC terminal labeling in pons

Single injections of anterograde dextran tracer into the mPFC of rats and rabbits resulted in multiple discrete clusters of punctate labeling in the pons, representing putative mPFC labeled axon terminals, that varied in number and density (e.g., Fig. 4). Relative density coefficients were determined for each discrete cluster of terminals (e.g., Fig. 4D–G), and were used to calculate the weighted COM for each system of terminal clusters in the pons observed for a given mPFC injection site (see Materials and Methods).

Rats

The loci of terminal clusters were primarily observed in the rostral one-third of the ipsilateral and contralateral pons in rat, most often in the medial to central region (Fig. 5A,C, left; four representative examples from individual injection sites distributed across the rostralcaudal axis are given in Fig. 6, 3D representations of all individual cases are shown in Fig. 8). Six out of nine cases revealed terminal fields ipsilateral to the mPFC injection site that were strikingly similar across individuals. These projection fields typically extended from the ventromedial edge of the pyramidal tract to the ventromedial surface of the pons, appearing roughly columnar in shape and ranging between 950 and 1,350 μm in length, and 620 to 900 μm at maximum width (e.g., Fig. 6B–D). These terminal clusters sometimes extended through the entire rostral half of the pons (600 μm), and appeared most dense at the rostral extent. Additional ipsilateral terminal fields were observed in these and the remaining three cases, and tended to be smaller and varied in shape, ranging from nearly spherical clusters with diameters of ~250 μm,

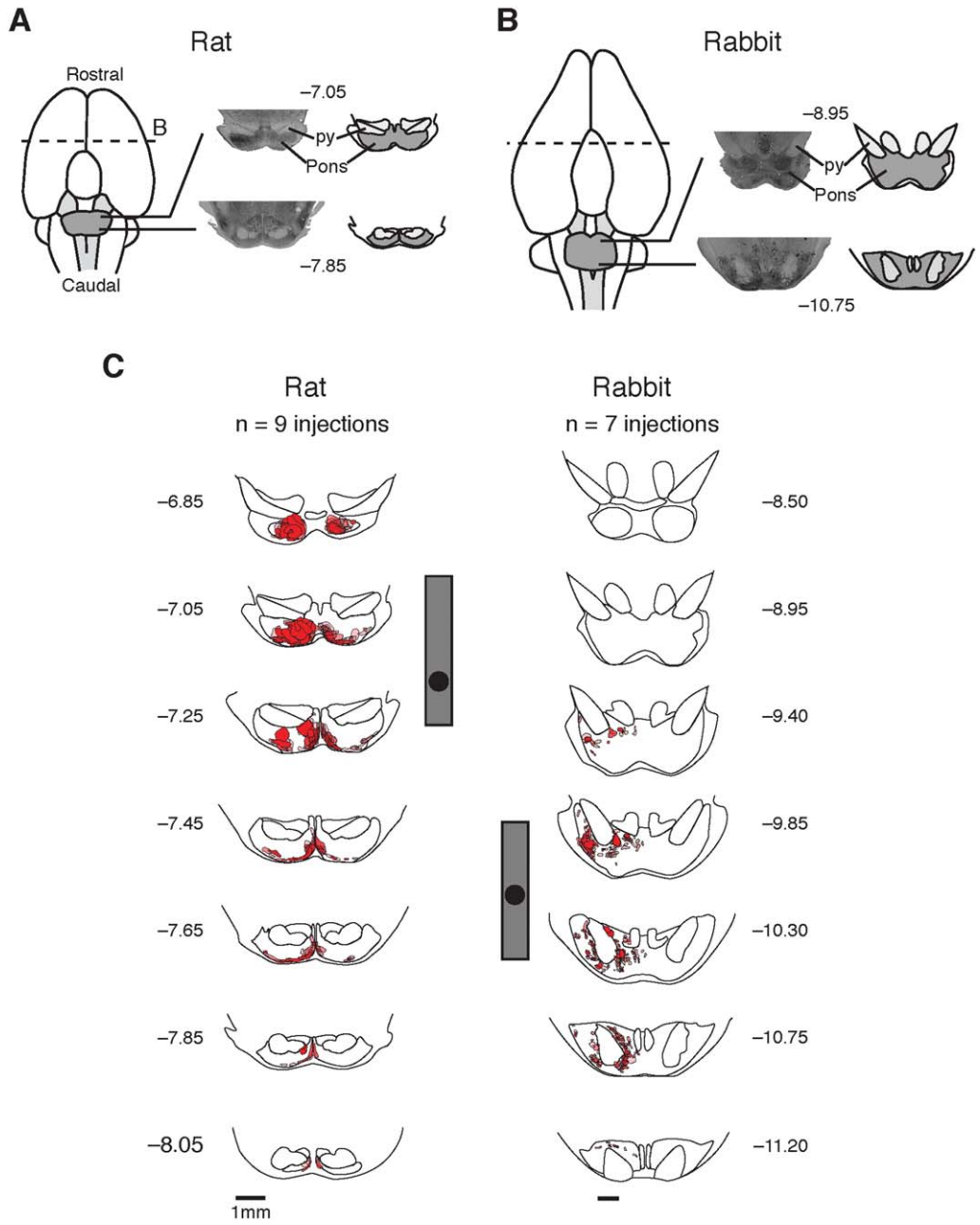

Figure 5. Schematics of the location of the pons and gross anatomical structure in rats and rabbits, and distribution of putative prefrontal terminals in the pons observed in each species. **A:** Representation of the rat brain (viewed from the ventral surface) showing the location of the pons (dark gray) and associated pyramidal tract (py, light gray). Coronal sections and line drawings from the more anterior (top) and posterior (bottom) pons are also shown (numbers indicate anterior-posterior stereotaxic coordinates relative to Bregma). **B:** Representation of the rabbit brain, as described for rats in A. **C:** Example coronal sections from along the rostrocaudal axis of the pons (numbers indicate stereotaxic coordinates relative to Bregma). Summation of the extent and density of prefrontal terminal clusters across all cases for rat and rabbit (shown in red). Boxplots (center) show the COM of labeled terminals (black markers) and IQR (gray box) for rats and rabbits. Note the difference in gross anatomical location of the pyramidal tract throughout the pons between rat and rabbit. Prefrontal terminals were preferentially labeled and were densest in the anterior pons of rats, while prefrontal terminals were observed at relatively more caudal locations surrounding the descending pyramidal tract in the intermediate pons.

to more elongated clusters 580 × 150 × 100 μm in length, width, and rostral-caudal extent, respectively (e.g., Fig. 6). Clusters of mPFC axon terminals were typically most dense in the ipsilateral pons, with contralateral labeling often appearing as a less dense "mirror image" of a subset of the ispilateral labeled terminals in 7/9 cases (e.g., arrow in Fig. 4C; Fig. 6B,C; Fig. 8 cases 2–7 and 9; contralateral labeling was not

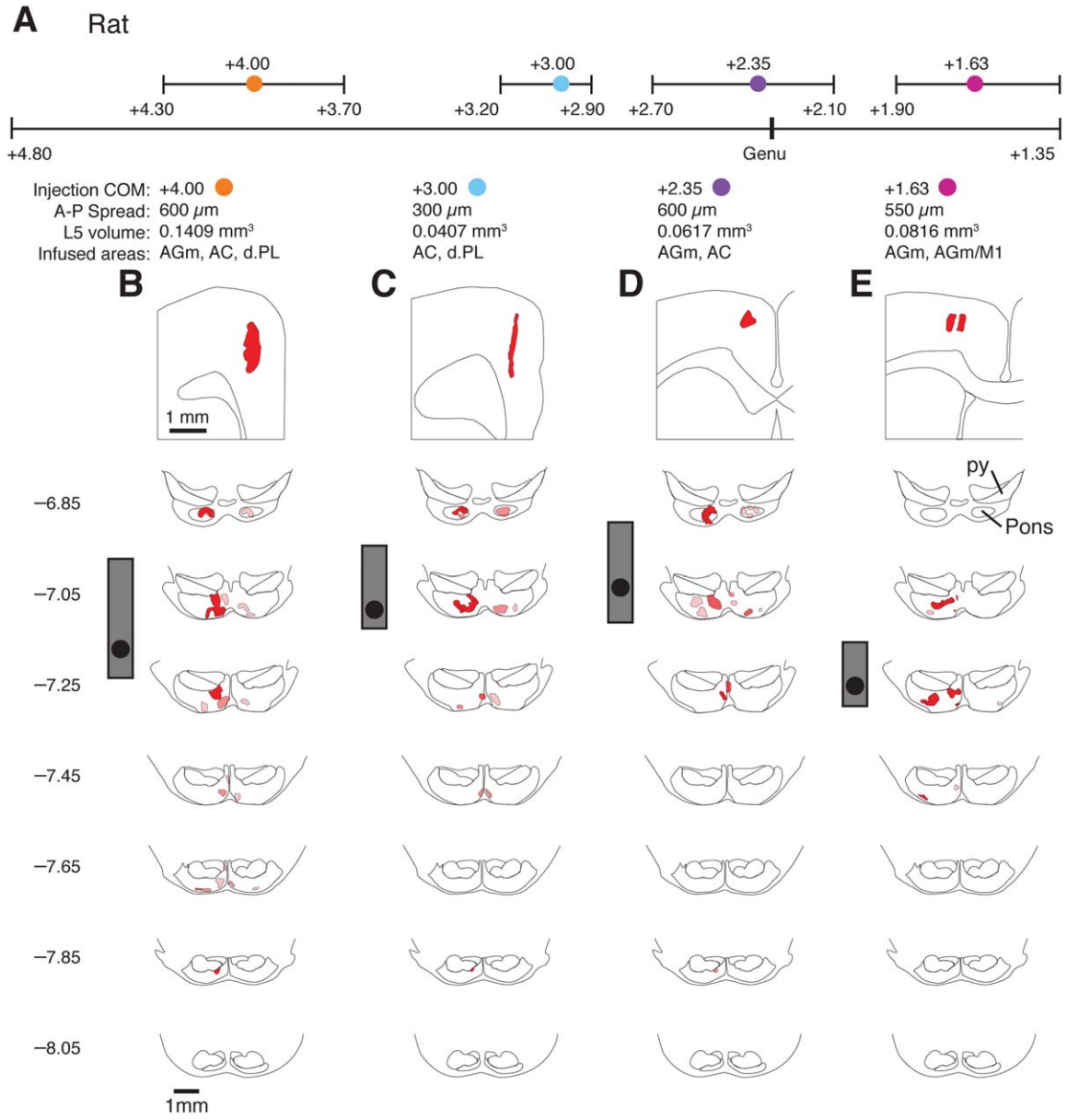

Figure 6. Prefrontal terminal labeling was observed in the rostral pons in all cases for rat, independent of the anterior-posterior coordinate or subregional location of labeled somata within the medial prefrontal cortex. **A:** Extent of labeled layer V tissue observed across cases in rat (bottom line), and the COM (colored markers) and IQRs of prefrontal labeled tissue for four individual cases (top; colors correspond to individual case assignments shown in 3D renderings in Figs. 8, 10A). **B–E:** Line drawings and general information (COM, anterior-posterior spread, Layer 5 volume and prefrontal subregion: AGm, medial agranular; AC, anterior cingulate; dPL, dorsal prelimbic; M1, primary motor cortex) of labeled layer V tissue (red) in the medial prefrontal cortex (top), and the prefrontal terminal labeling observed for that injection (below). Anterior-posterior stereotaxic coordinates (relative to Bregma) and COM ± IQR calculated for each example are given.

observed in two cases, Fig. 8 cases 1 and 8). Contralateral clusters of terminals varied in size and shape, but tended to be more ellipsoidal than corresponding columns of ipsilateral labeling (they appeared to lack the dorsal component that was most proximal to the pyramidal tract). The largest contralateral terminal clusters were ~850 μm in length by 300 μm in width by 250 μm in rostral-caudal extent. Smaller clusters of labeled terminals were ~200 × 150 × 100 μm. The ipsilateral pyramidal tract is assumed to be the source of contralateral labeling, given that no labeling was observed in the pyramidal tract contralateral to the mPFC injection site (e.g., Fig. 4C, double-asterisk).

In 8/9 cases terminal labeling was observed in the rostralmost 100 μm of the rat pons (Fig. 5C, left; the exception is shown in Fig. 6E). The COM of terminal

clusters in the pons resulting from each mPFC injection site was located in the rostral 400 μm of the pons in 8/9 cases in the rat (e.g., Fig. 6B–E, black markers). The IQRs of weighted terminal clusters for these injections sites were also restricted to the rostral 400 μm and substantially skewed toward the rostral pole relative to the COM, indicating that 75% of mPFC terminals were observed in the rostral pons in rats (e.g., Fig. 6B–E, boxplots; 3D data shown in Fig. 8 for all individual cases and cumulatively in Fig. 10A). An exception to this pattern was observed in three cases, which in addition to dense rostral labeling also displayed a relatively small but dense region of terminal labeling that was typically restricted to the medial wall and ventral aspect of the pons along nearly the entire rostrocaudal extent of the structure (Fig. 8, cases 2–4). The only difference noted between the injection sites in these versus other cases was labeling at or near the dorsal PL – ventral AC border. Interestingly, there were no discernable differences in the patterns of putative terminals in the pons resulting from rostral versus caudal mPFC injection sites in the rat—the pons labeling from more rostral mPFC infusions were remarkably similar to that observed for more caudal infusion sites (e.g., Figs. 6, 8). Additionally, no systematic differences in mPFC corticopontine projection patterns were observed between anterograde tracer injections in the different subregions of mPFC sampled in this study, with the possible exception described above.

Rabbits

In contrast to rats, the loci of clusters of mPFC terminals was observed in the intermediate region of the ipsilateral pons of the rabbit, most often in close association with the pyramidal tract as it descends ventrally and medially through the pons (Fig. 5C, right, and Figs. 9, 10B). Terminal clusters in the rabbit were often more elliptical, in further contrast to the columnar shape of the most dense mPFC terminal clusters in the rat pons. In 5/7 cases the largest and densest clusters of terminals were observed in the areas immediately medial or lateral to the ventral pyramidal tract (Figs. 5C, left, Fig. 7). The dimensions of these mPFC terminal clusters ranged from 500–1,100 μm in length and 450–700 μm in width, and typically extended 400–750 μm in the anterior-posterior axis. Smaller clusters of varying density were also observed distributed throughout the mediodorsal and lateral pons. These clusters ranged in size from 150–180 μm and 300–250 μm in length and width, respectively, and extended 250–500 μm in the rostral-caudal axis. Although single axons were occasionally observed exiting the pyramidal tract and crossing the midline to the contralateral hemisphere, clusters of labeled terminals were not observed in the contralateral rabbit pons for any of the mPFC injections (Fig. 7B–E; Figs. 9, 10B).

Clusters of mPFC terminals were not observed in the most rostral 800 μm of the rabbit pons (Fig. 5C, left). Instead, mPFC terminals were restricted to the intermediate pons in 7/7 cases, and typically showed clusters of terminals that were distributed symmetrically around the COM along the rostral-caudal axis (Fig. 7B–E, black markers and boxplots). Patterns of pontine terminal labeling were not different between caudal and rostral mPFC injection sites in rabbit, similar to the finding in rat (compare Fig. 7B,C to 7E; Fig. 9). Likewise, no systematic differences in projection patterns were observed between anterograde tracer injections in the different subregions of mPFC sampled in this study.

Comparison of mPFC projection patterns between rats and rabbits

A collapsed summary of all labeled terminals observed in the pons for rat and rabbit is given in Figure 5C and a 3D summary in Figure 10. The loci of the clusters of mPFC terminals from all rats was biased toward the rostral pole of the rat pons, while the rostral pons of rabbits was devoid of mPFC terminal clusters, even though there was substantial overlap in the relative mPFC regions of anterograde tracer uptake by layer V cells between rats and rabbits (Figs. 1, 3, 10). Some mPFC terminal labeling was observed in the intermediate pons of rats that overlapped with the locus of terminal labeling in the rabbit pons, but comprised less than 25% of all mPFC terminal clusters in the rat pons (Fig. 5C). In Figure 10, species-specific prefrontal terminal labeling in the medial pons can be compared when each species is viewed from an anterior perspective (Pons, top image), while differences in terminal labeling in the rostral pons is best noted from a ventral perspective (Pons, bottom image). A striking difference in mPFC corticopontine projections between the two species is the substantial contralateral labeling observed in most cases in rat, which was completely absent in rabbit (Figs. 5–10).

DISCUSSION

The patterns of mPFC projections to the pons were characterized for rat and rabbit using anterograde tracing techniques. There were striking differences in the distribution of labeled prefrontal axon terminals between the two species. Both the overall topography of projections across the rostral-caudal axis and the degree of contralateral labeling observed differed between rats and rabbits.

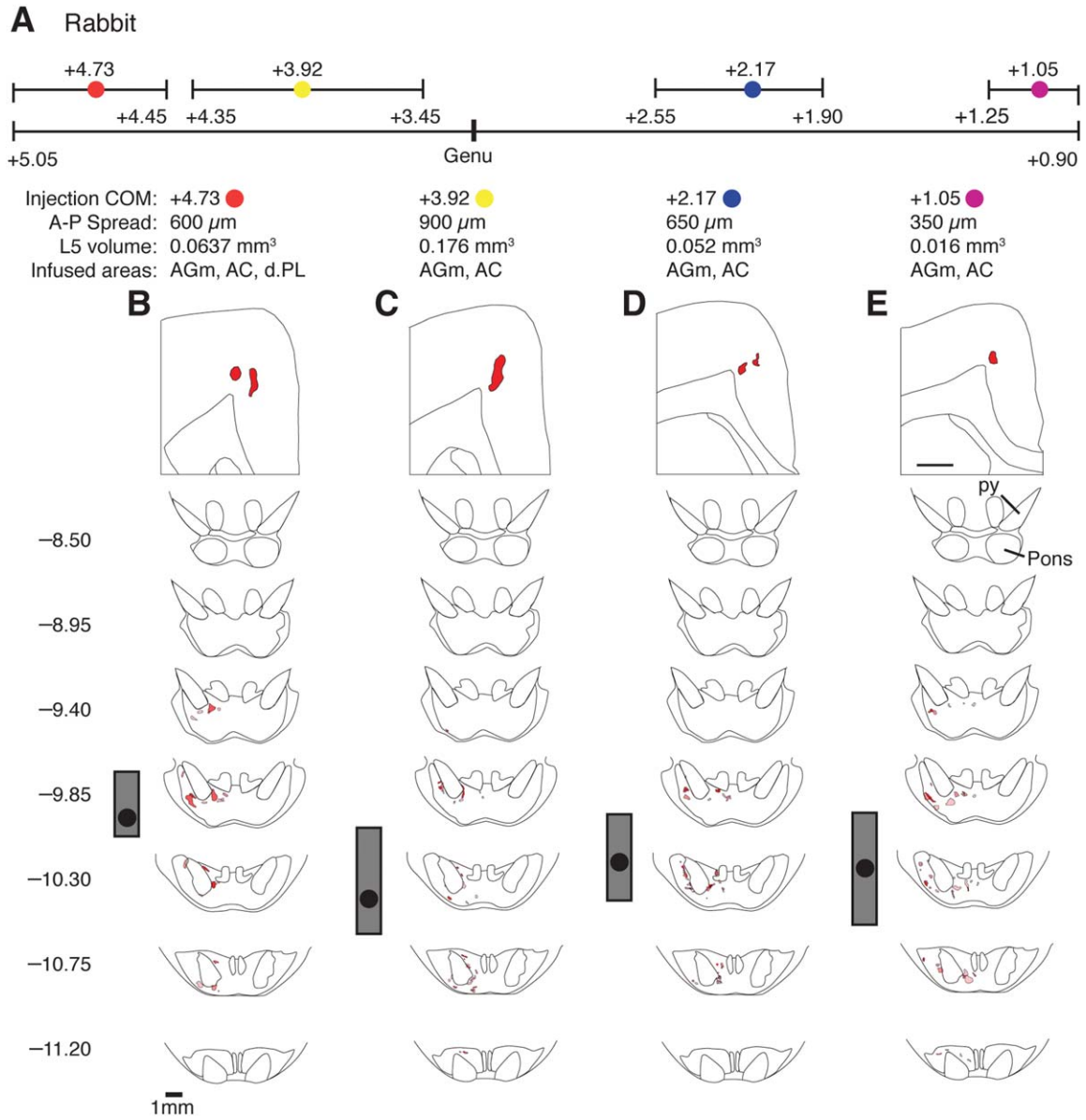

Figure 7. Prefrontal terminal labeling was observed in the intermediate to more caudal pons in all cases for rabbit, independent of the anterior-posterior coordinate or subregional location of labeled somata within the medial prefrontal cortex. **A:** Extent of labeled layer V tissue observed across cases (bottom line), and the COM (colored markers) and IQRs of prefrontal labeled tissue for four individual cases (top; colors correspond to individual case assignments shown in 3D renderings in Figs. 9, 10B). **B–E:** Line drawings and general information (as described in Fig. 6) of labeled layer V tissue (red) in the medial prefrontal cortex (top), and the prefrontal terminal labeling observed for that injection (below). Anterior-posterior stereotaxic coordinates (relative to Bregma) and COM ± IQR calculated for each example are given.

Species-specific differences in the rostral-caudal distributions of mPFC corticopontine terminals

More than 75% of mPFC labeled terminals in rat were observed in the rostral half of the medial pons, often extending from the ventromedial pyramidal tract toward the ventral surface of the pons (Figs. 5C, left, and 10A). In contrast, the rostral pons of rabbit was entirely devoid of mPFC labeled terminals (Figs. 5C, right, and 10B). Instead, mPFC corticopontine terminals in rabbit tended to surround the pyramidal tract as it descended ventromedially through the pons over the intermediate rostral-caudal extent (Fig. 10).

It is unlikely that the species-specific divergence in mPFC corticopontine projections demonstrated here could be explained by potential anterior-posterior differences in the coordinates of the mPFC injection sites between the rats and rabbits used for this study. First,

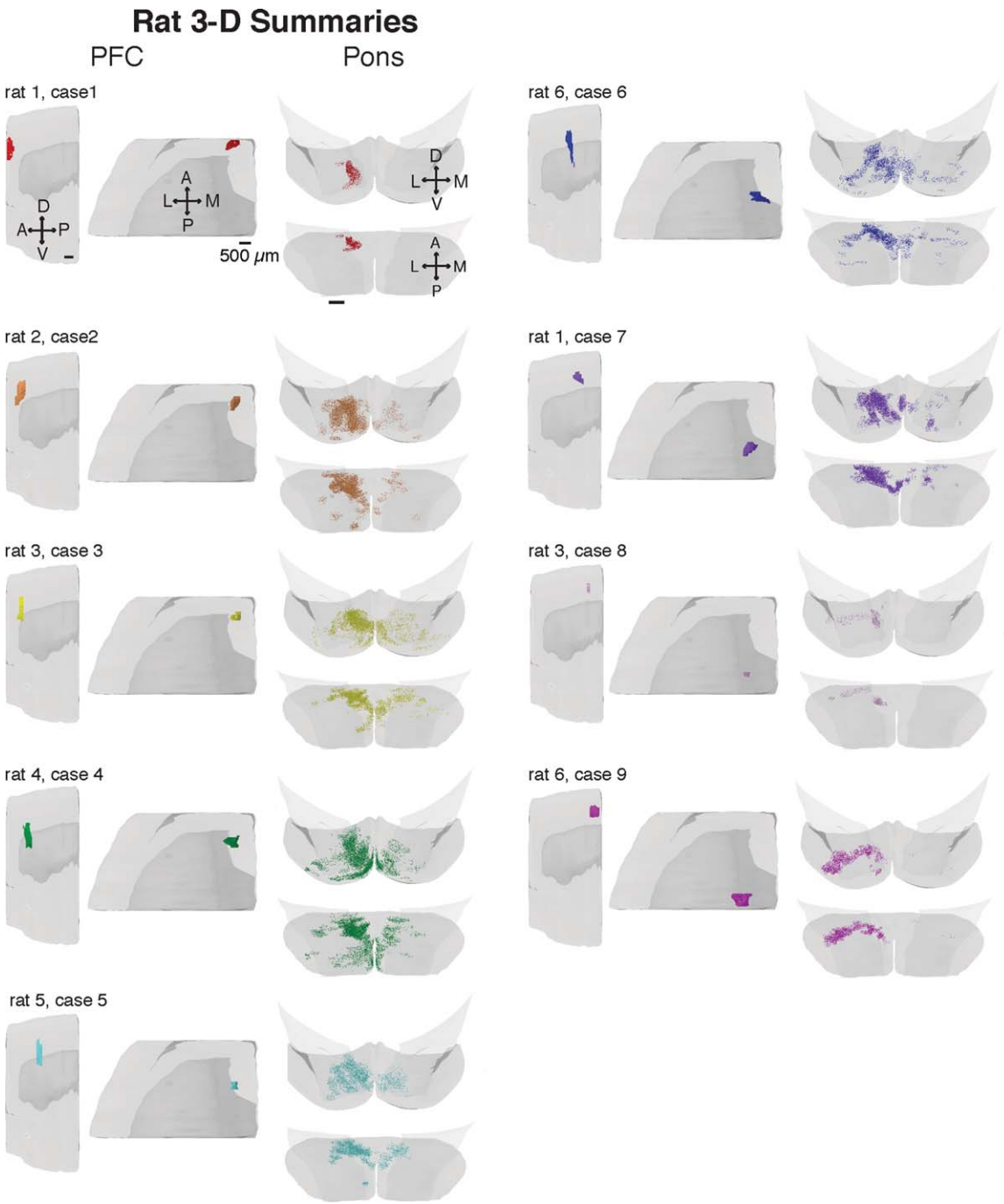

Figure 8. Three-dimensional reconstructions of labeled layer V tissue resulting from tracer injection in mPFC and associated terminal labeling in the pons for each rat. Cases are ordered from most rostral to the most caudal prefrontal injection site (as columns running from top to bottom). Two perspectives are shown for each injection site (PFC, left) and for each reconstructed pons (right). Directional compasses as described in Figure 2. The patterns of terminal labeling in the rostromedial pons were not different across cases depending on anterior-posterior location of prefrontal injection sites. Terminal labeling in the medial pons across cases can be compared when viewed from an anterior perspective (Pons, top image), while terminal labeling in the rostral pons across cases is best noted from a ventral perspective (Pons, bottom image).

the locations of mPFC injection sites in the rats and rabbits overlapped considerably in a relative anterior-posterior axis (by ~75%; Figs. 1, 3), while the overlap of mPFC terminals in the pons showed very little overlap (<25%; Figs. 5C, 10). Second, the species-specific differences are still observed when only mPFC injections within the same relative rostral-caudal extent are considered (injections between +1.0–3.5B in rats and

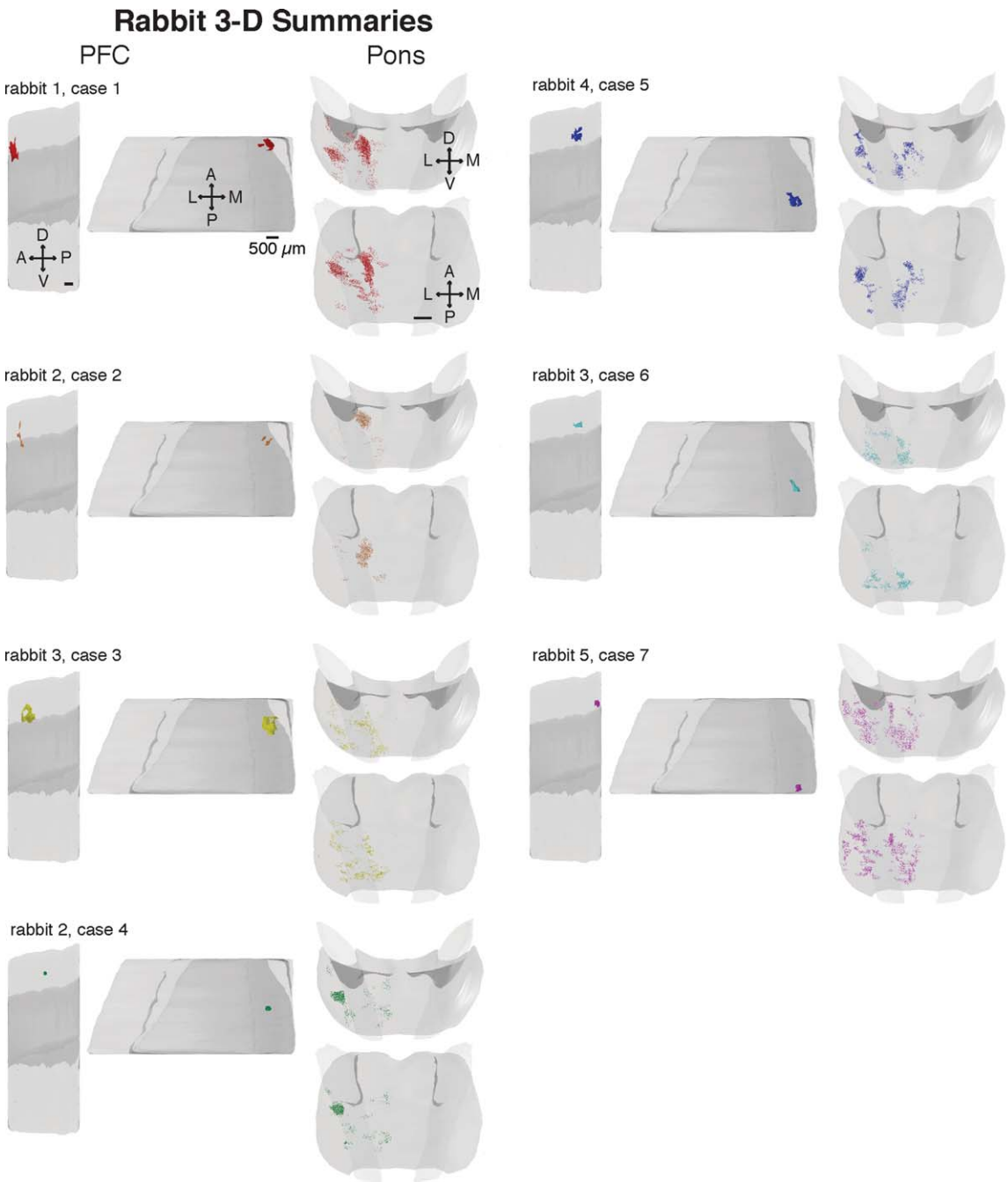

Figure 9. Three-dimensional reconstructions of labeled layer V tissue from prefrontal (PFC) tracer injection and associated terminal labeling in the pons for each rabbit. Cases are ordered from most rostral to the most caudal prefrontal injection site (as columns running from top to bottom). Two perspectives are shown for each injection site (PFC, left) and for each reconstructed pons (right). Directional compasses as described in Figure 2. The patterns of terminal labeling in the intermediate to caudal pons were not different across cases depending on anterior-posterior location of prefrontal injection sites. Terminal labeling in association with the descending pyramidal tract is clearly observed from both anterior (Pons, top image) and ventral perspectives (Pons, bottom image).

+2.0–5.0B in rabbits, Fig. 3; compare individual rats from Fig. 6C–E to individual rabbits given in Fig. 7C,D). Finally, injections made at various locations along the anterior-posterior extent of the mPFC did not reveal distinct patterns of pontine terminal labeling within species (Fig. 6B–E for rat, Fig. 7B–E for rabbit), and so any rostral-caudal differences in the injection sites between the rats and rabbits is unlikely to explain the species-specific results. Furthermore, data from previous studies in which more caudal rat mPFC injections or more

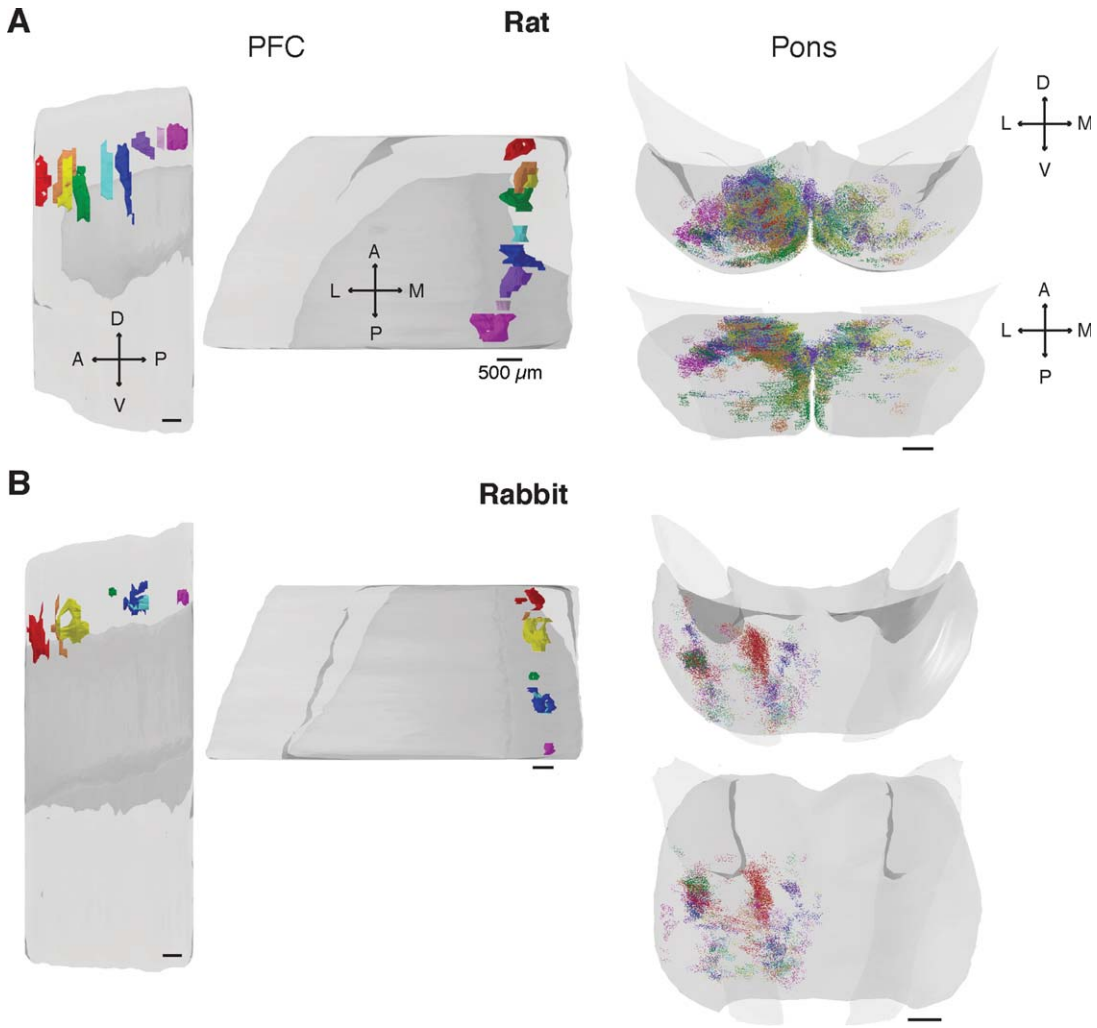

Figure 10. Summary of medial prefrontal labeled layer V tissue resulting from injection of anterograde label, and the pattern of putative terminal labeling in the pons in rat (**A**) and rabbit (**B**). Three-dimensional perspectives and compass directions are as described for Figures 8 and 9. Note the species-specific patterns of prefrontal terminal labeling observed between rat and rabbit even though overlapping regions of medial prefrontal cortex were labeled for the two species. The medial prefrontal cortex of rats preferentially projects to the rostromedial pons, while the mPFC of rabbits preferentially projects to pontine regions that surround the pyramidal tract as it descends ventromedially through the intermediate to more caudal pons.

rostral rabbit mPFC injections resulted in similar patterns of pons terminal labeling as reported here (Wiesendanger and Wiesendanger, 1982b; Buchanan et al., 1994). Together, the evidence strongly suggests that differences in the pattern of mPFC projections reported here between rat and rabbit represent a species-specific divergence in the topography of corticopontine projection patterns.

Species-specific differences in contralateral mPFC corticopontine projections

This comparative study revealed contralateral projections from mPFC to the pons in rat that were not observed in rabbit. Discrete clusters of labeled mPFC terminals were observed in the rostromedial region of the contralateral pons in rat, often mirroring the pattern of terminal clusters observed on the ipsilateral side. In contrast, clusters of labeled terminals were never observed in the contralateral pons of rabbit (Figs. 5, 7, 9, 10). It should also be noted that labeled axons were never observed in the contralateral pyramidal tract, so it is presumed that labeled axons from the ipsilateral pyramidal tract crossed the midline and formed terminal clusters in the contralateral pons in the rat. Given the absence of labeled axons in the contralateral pyramidal tract, it is unlikely that uptake of the anterograde tracer by callosally projecting fibers could have resulted in apparent contralateral labeling. In the rabbit, single axons were occasionally observed crossing the

midline but did not give rise to terminal clusters in the contralateral pons. It is possible that these axons contributed to very sparse or dispersed contralateral terminal labeling in rabbit that was not detected by our analysis. However, the presence of diffusely labeled terminals in the contralateral pons of rabbit would still be in sharp contrast to the readily apparent terminal clusters observed in the contralateral pons of rat.

Qualifications for the current study

The proportion of labeled tissue relative to mPFC volume appeared smaller in the rabbit, despite the fact that considerably more tracer was injected. This would likely still be true even if our analysis underestimated the volume of labeled tissue at the injection sites. Therefore, proportionally less of the mPFC was sampled in rabbit than in rat, which included unsampled regions within the rostrocaudal extent (Fig. 3). Therefore, it is possible that unsampled mPFC regions in rabbit may have shown rostral or contralateral labeling in the pons. This seems unlikely, given that rostral and caudal extents of the same mPFC subregions showed largely overlapping and entirely ipsilateral terminal labeling, but cannot be ruled out in this study.

Comparison of findings to previous work

The current study both supported and further refined previous work examining the specific pattern of pontine projections from the mPFC in rats and rabbits by using more spatially restricted anterograde tracer injections, and by further defining injection sites relative to labeled layer V tissue. Furthermore, we allowed for direct comparisons between rat and rabbit, and revealed substantial species-specific differences in the topography of mPFC corticopontine projection patterns. The pattern of mPFC to pons projections demonstrated here is in general agreement with the overall topography of inputs from frontal cortical regions to the rostromedial pons previously reported for rat (Wiesendanger and Wiesendanger, 1982a,b; Leergaard and Bjaalie, 2007). More specifically, the relative restriction of mPFC terminals to the rostral half to one-third of the medial pons, in addition to distinct contralateral labeling, was also reported in prior studies (Domesick, 1969; Wiesendanger and Wiesendanger, 1982b; Wyss and Sripanidkulchai, 1984; Leergaard and Bjaalie, 2007). The overall pattern of mPFC to pons projections in rat is similar to that demonstrated for monkey (Vilensky and Van Hoesen, 1981; Schmahmann and Pandya, 1997b) and cat (Brodal and Bjaalie, 1992), and is in sharp contrast to that observed for rabbit. We noted mPFC terminal fields immediately surrounding the pyramidal tract as it descended ventromedially through the intermediate anterior-posterior extent of the pons in rabbit, which were not observed in the rostral or contralateral pons. Although early reports showed frontal cortical terminal fields restricted to the dorsal and medial peduncular pons in rabbit (Abdel-Kader, 1968), the pattern of mPFC inputs reported here is consistent with more recent investigations that focused on corticopontine inputs specifically from the mPFC (Buchanan et al., 1994; Weible et al., 2007; Siegel et al., 2012).

Similarities in corticopontine projections between rat and rabbit

The ability to localize injection sites to layer V cells (the well-established source of corticopontine inputs; e.g., Legg et al., 1989) allowed for more precise localization of mPFC cells that were the source of terminal labeling in the pons. Interestingly, mPFC injection sites at different anterior-posterior coordinates did not reveal distinct mPFC corticopontine projection patterns within species (i.e., compare Fig. 6B–E across rats, compare Fig. 7B–E across rabbits). Similarly, there were no consistent differences in the location of labeled terminals between the mPFC subregions sampled here within either species. This was also true for the anterior and posterior extents of the same mPFC subregion, particularly rostral and caudal AC (rat: compare injection sites from rat 1, Fig. 8; rabbit: compare injection sites from rabbit 3, Fig. 9), which the data suggest can play different functional roles (Kronforst-Collins and Disterhoft, 1998; Hattori et al., 2010). An exception may exist in rat for the two most caudal injections (between +2.0 and +1.35B, one of which is shown in Fig. 6E). Medial PFC projections were not observed at the rostralmost pole in these two cases, and showed little if any contralateral labeling. Although previously reported for rat (Domesick, 1969; Wyss and Sripanidkulchai, 1984), the generally indistinguishable patterns of mPFC corticopontine terminal labeling across these dimensions within species is particularly compelling given the highly restricted and spatially segregated injection sites in the current study, even if separated by 2 mm or more in the anterior-posterior axis.

An additional similarity between rat and rabbit was that for individual injection sites, we observed multiple discrete patches of mPFC labeled terminals distributed over a restricted pontine region. This topographically constrained yet highly divergent pattern is similar to previous reports of corticopontine projections in all species studied (Abdel-Kader, 1968; Wiesendanger and Wiesendanger, 1982b; Brodal and Bjaalie, 1992; Leergaard and Bjaalie, 2007). It has been speculated that each patch represents a "private" or isolated line of

input from a fairly restricted area of cortex, and that the distribution of patches from a given input source serves to ensure that the information from the cortical input source reaches expansive regions of cerebellar cortex (reviewed in Wiesendanger and Wiesendanger, 1982b; Brodal and Bjaalie, 1992). More controversial is the degree to which inputs near the borders of adjacent terminal patches may converge onto the same pontine neurons, the output of which would reflect some integration of those inputs (Wiesendanger and Wiesendanger, 1982b; Kosinski et al., 1988; Brodal and Bjaalie, 1992; but see Schwarz and Möck, 2001; Schwarz et al., 2005). Putative convergence of corticopontine inputs has been substantiated with double-anterograde tracer studies in cat demonstrating some partial overlap of adjacent terminal fields from distinct cortical regions (Bjaalie and Brodal, 1989; Brodal et al., 1991). The functional integration of inputs from different cortical regions has been suggested by single-unit electrophysiological studies in cat, monkey, and rat demonstrating the ability to evoke spike activity when stimulating distinct but nearby cortical regions in nearly half of sampled pontine projection cells (Rüegg and Wiesendanger, 1975; Rüegg et al., 1977; Potter et al., 1978). Although the data presented here do not address this issue, its consideration is essential in order to determine the possible impact of the different topographies of mPFC to pons projection patterns observed between rat and rabbit. However, it should be noted that if a complete lack of convergence between adjacent terminal fields in the rat and rabbit pons were to be demonstrated it would suggest that the general role of the pons would be more similar to that of a relay station. Such a finding presumes that pontine neurons would simply pass on information regarding upstream spike activity without any integration of those inputs, making the exact topography of corticopontine projections of little functional relevance. Even so, the species-specific differences reported here would continue to be of considerable interest from a developmental perspective (O'Leary et al., 1991; Leergaard et al., 1995).

Functional impact of species-specific differences in corticopontine projections

It is hypothesized that any integration of inputs in the pons would only occur at the putative overlapping borders of adjacent terminal fields. Thus, species-specific differences in corticopontine projection patterns could result in the integration of different cortical inputs depending on what other brain areas project to the same region of the pons in that species. It should be noted that the general corticopontine mapping described for various species is an acknowledged over-simplification, with terminal patches also commonly observed outside of the general projection region (Wiesendanger and Wiesendanger, 1982b; Leergaard and Bjaalie, 2007). Nevertheless, the broad topographical organization of corticopontine inputs established for rat predicts that the greatest opportunity for integration with mPFC inputs would occur with input from rostromedial primary motor areas (such as frontal eye field, whisker, and potentially forelimb primary and supplementary motor cortex regions; Wiesendanger and Wiesendanger, 1982a; Kosinski et al., 1986; Guandalini, 2001; Alloway et al., 2010) and the rostralmost subregions of primary somatosensory cortex (such as barrel cortex and possibly forelimb; Wiesendanger and Wiesendanger, 1982a; Kosinski et al., 1986; Alloway et al., 2010). Corticopontine input from auditory, visual, retrosplenial, and caudal or lateral somatosensory regions would be least likely to be directly integrated with mPFC input given that the terminal fields from those structures tend to lie far lateral or in the caudal half of the pons in rat (Wiesendanger and Wiesendanger, 1982a,b; Azizi et al., 1985; Schwarz et al., 2005; Leergaard and Bjaalie, 2007).

Although a broad topographical organization for rabbit corticopontine projections is far less established, the available data suggest similarities with rat in that there would be the highest opportunity for integration with primary motor regions, and less so for auditory and visual cortical input (Abdel-Kader, 1968; Wells et al., 1989; Knowlton et al., 1993). A notable distinction between the potential for the integration of inputs in the pons between rat and rabbit is the apparent topographical overlap of mPFC terminal fields in rabbit with input from somatosensory and retrosplenial cortices (according to the map of Abdel-Kader, 1968). A second distinction is the putative overlap of mPFC corticopontine inputs with that of the deep layer, multimodal region of the superior colliculus in rabbit (Wells et al., 1989), while in rat inputs from the deep layers of the super colliculus are restricted to the caudolateral pons (Burne et al., 1981) and do not appear to overlap topographically with mPFC inputs in the rat pons. With the exception of auditory and visual corticopontine inputs, it appears that mPFC inputs in rabbit tends to violate a confined topographical projection pattern in that it surrounds and extends from the descending pyramidal tract, while other cortical inputs are reported to remain more restricted within their respective dorsal, lateral, or ventromedial borders relative to the peduncle. Overall, the available data suggest that mPFC corticopontine input in rabbit is generally more likely to be integrated with input from somatosensory and associational brain regions than would be predicted in rat.

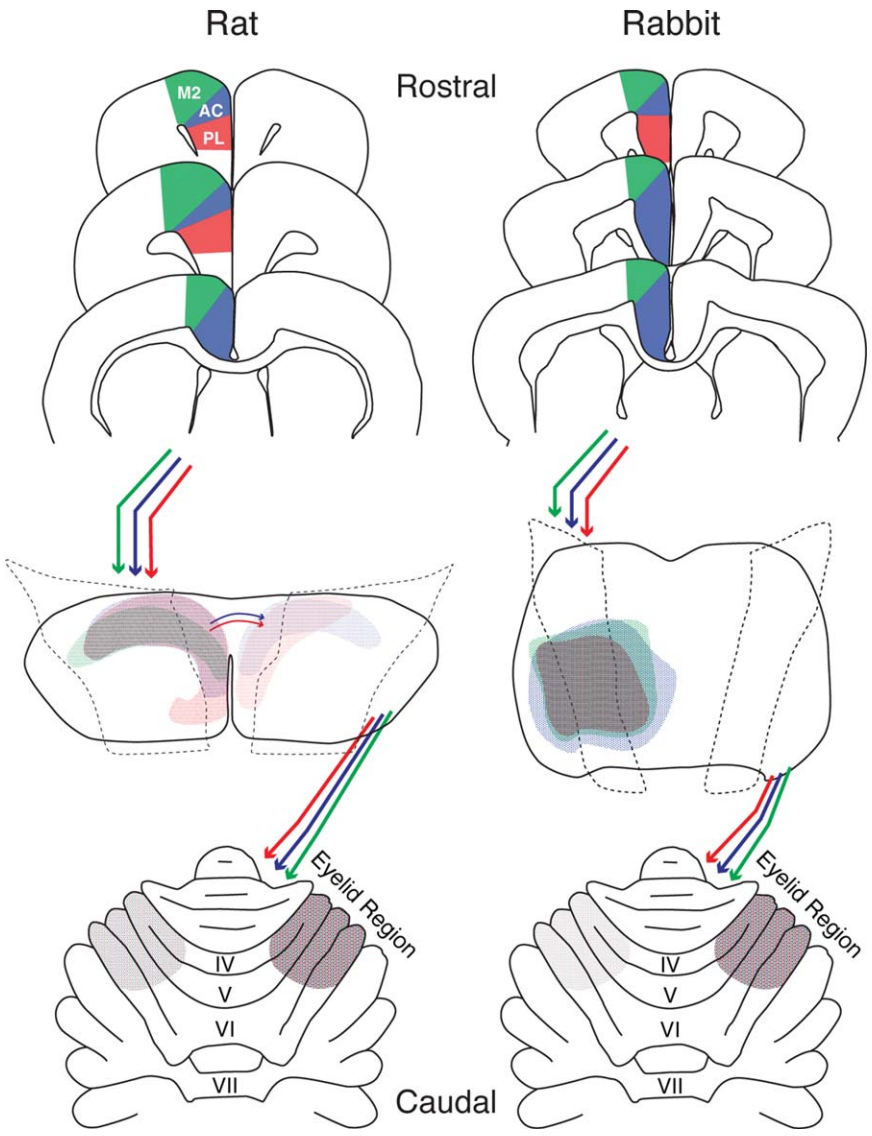

Figure 11. Schematic of prefrontocerebellar projection pathway in rats (left) and rabbits (right), with colors indicating projection sites for the subregions of mPFC throughout the pathway (green: medial agranular, blue: anterior cingulate, red: prelimbic). Note that the rostral and caudal extents of a given subregion projected to largely overlapping pontine regions (see text). In rat, the current study demonstrates that mPFC subregions project to the ipsilateral and less densely to the contralateral rostromedial pons via the ipsilateral pyramidal tract. Previous work has shown that the ipsilateral and contralateral pons each project predominantly to the opposite cerebellar hemisphere and modestly to the same hemisphere, including the anterior portion of Lobules V/VI that support eyeblink conditioning (see text). In rabbit, the mPFC projects ipsilaterally to the intermediate/caudal peduncular pons, which then projects predominantly to the contralateral cerebellar hemisphere and modestly to the same hemisphere, including cerebellar cortex regions that support eyeblink conditioning. Note that pontocerebellar projections in both species actually project expansively across cerebellar lobules, and are not indicated here (Brodal and Bjaalie, 1992).

Implications of species-specific differences in prefrontopontine projections for trace eyeblink conditioning

The primary motivation for the current study was to investigate the possibility of species-specific differences in prefrontopontine input patterns between rabbit and rat as it relates to trace eyeblink conditioning. The mPFC and cerebellum have been shown to be necessary for the expression of trace conditioned responses in both species (e.g., Kronforst-Collins and Disterhoft, 1998; Takehara et al., 2003; Kalmbach, 2008), with prefrontal inputs reaching the cerebellum via the pons. In rats, experiments focusing on the mPFC would likely require bilateral manipulation, assuming that both

hemispheres would receive stimulus-associated inputs from presentation of a tone or light CS. Because mPFC inputs to the pons are unilateral in rabbits, bilateral manipulation should be unnecessary. Clearly, different regions of the pons would be predicted to support trace conditioning in rats and rabbits based on the current study. As such, manipulations of mPFC inputs to the cerebellum should be bilateral and focused on the rostromedial pons in rats, and in the intermediate to caudal peduncular region unilaterally in rabbits (Fig. 11). A putative role for the rostromedial pons in trace eyeblink conditioning has not been tested in rat, but unilateral infusions of muscimol in the intermediate lateral pons in rabbit, located just adjacent to the peduncle, can abolish trace conditioned responses (Kalmbach et al., 2009).

Projections from the pons to the cerebellum are predominantly, but not exclusively, to the contralateral cerebellar hemisphere in both species (Mihailoff, 1983; Yeo et al., 1985; Serapide et al., 2001; Tracy et al., 2013). Importantly, the rostromedial pons in rat and the intermediate peduncular pons in rabbit both include projections to cerebellar lobules V/VI (Fig. 11; Mihailoff, 1983; Yeo et al., 1985b; Serapide et al., 2001; Tracy et al., 2013), which are the established regions of cerebellar cortex shown to support eyeblink conditioning in rabbits and rats (Yeo et al., 1985a; Garcia et al., 1999; Plakke et al., 2007; Kalmbach et al., 2010). Because eyeblink conditioning does not require bilateral coordination (only one eye is typically trained) there is likely little implication of unilateral versus bilateral inputs at the level of the cerebellum for this learning paradigm, except perhaps under specific circumstances. For example, if after acquisition training is switched to the opposite eye, one might expect accelerated learning because the opposite cerebellar hemisphere would not be naïve to the CS. In support, Yeo et al. (1985a) found that post-learning lesions of cerebellar lobule HVI abolished CRs, but that rabbits relearned quickly when the opposite eye was trained with the same CS. However, eyeblink conditioning could be used to test the functional nature of the prefrontopontine contralateral projection in rat using microstimulation of the mPFC ipsilateral to the trained eye as the CS (learned behavior would be mediated by the ipsilateral cerebellum, which under these conditions would only receive the more modest prefrontal inputs to the contralateral pons). Because the prefrontocerebellar input is bilateral, rats should be able to learn independently of which hemisphere is stimulated, while the unilateral nature of the prefrontocerebellar pathway in rabbits should preclude learning if the ipsilateral mPFC is stimulated.

CONFLICT OF INTEREST

The authors state no identified conflict of interest regarding the current work.

AUTHOR CONTRIBUTIONS

All authors had full access to all the data in the study and take responsibility for the integrity of the data and the accuracy of the data analysis, and have read and revised the submitted article. Study concept and design: JJS, RAC, ND, BEK, MVM. Acquisition of data: JJS, RAC, MVM, EDM. Analysis and interpretation of data: RAC, JJS, MVM, EDM. Drafting of the article: JJS, MVM, RAC. Statistical analysis: JJS, MVM. Administrative, technical, and material support: EDM. Project supervision: RAC, JJS, and DJ.

REFERENCES

Abdel-Kader GA. 1968. The organization of the cortico-pontine system of the rabbit. J Anat 102:165–181.

Alloway KD, Smith JB, Beauchemin KJ. 2010. Quantitative analysis of the bilateral brainstem projections from the whisker and forepaw regions in rat primary motor cortex. J Comp Neurol 518:4546–4566.

Azizi SA, Burne RA, Woodward DJ. 1985. The auditory corticopontocerebellar projection in the rat: inputs to the paraflocculus and midvermis. An anatomical and physiological study. Exp Brain Res 59:36–49.

Bjaalie JG, Brodal P. 1989. Visual pathways to the cerebellum: segregation in the pontine nuclei of terminal fields from different visual cortical areas in the cat. Neuroscience 29:95–107.

Brodal P, Bjaalie JG. 1992. Organization of the pontine nuclei. Neurosci Res 13:83–118.

Brodal P, Bjaalie JG, Aas J-E. 1991. Organization of cingulo-ponto-cerebellar connections in the cat. Anat Embryol 184:245–254.

Buchanan S, Thompson R, Maxwell B, Powell DA. 1994. Efferent connections of the medial prefrontal cortex in the rabbit. Exp Brain Res 100:469–483.

Burne RA, Azizi SA, Mihailoff GA, Woodward DJ. 1981. The tectopontine projection in the rat with comments on visual pathways to the basilar pons. J Comp Neurol 202: 287–307.

Clark GA, McCormick DA, Lavond DG, Thompson RF. 1984. Effects of lesions of cerebellar nuclei on conditioned behavioral and hippocampal neuronal responses. Brain Res 291:125–136.

Clark RE, Manns JR, Squire LR. 2002. Classical conditioning, awareness, and brain systems. Trends Cogn Sci (Regul Ed) 6:524–531.

Diamond A. 2000. Close interrelation of motor development and cognitive development and of the cerebellum and prefrontal cortex. Child Dev 71:44–56.

Dobson CC, Mongillo DL, Poklewska-Koziell M, Winterborn A, Brien JF, Reynolds JN. 2012. Sensitivity of modified Bielmaze task, compared with Y-maze task, to measure spatial learning and memory deficits of ethanol teratogenicity in the guinea pig. Behav Brain Res 233:162–168.

Domesick VB. 1969. Projections from the cingulate cortex in the rat. Brain Res 12:296–320.

Fiala JC. 2005. Reconstruct: a free editor for serial section microscopy. J Microsc 218:52–61.

Freeman JH, Rabinak CA. 2004. Eyeblink conditioning in rats using pontine stimulation as a conditioned stimulus. Integr Physiol Behav Sci 39:180–191.

Glover JC, Petursdottir G, Jansen JKS. 1986. Fluorescent dextran-amines used as axonal tracers in the nervous system of the chicken embryo. J Neurosci Methods 18: 243–254.

Guandalini P. 2001. The efferent connections to the thalamus and brainstem of the physiologically defined eye field in the rat medial frontal cortex. Brain Res Bull 54:175–186.

Hattori S, Yoon T, Disterhoft JF, Weiss C. 2014. Functional reorganization of prefrontal cortical network mediating consolidation of trace eyeblink conditioning. J Neurosci 34:1432–1445.

Jones BF, Groenewegen HJ, Witter MP. 2005. Intrinsic connections of the cingulate cortex in the rat suggest the existence of multiple functionally segregated networks. Neuroscience 133:193–207.

Kalmbach BE. 2008. Forebrain-cerebellum interactions revealed by trace eyelid conditioning. Houston: University of Texas Graduate School of Biomedical Sciences at Houston.

Kalmbach BE, Ohyama T, Kreider JC, Riusech F, Mauk MD. 2009. Interactions between prefrontal cortex and cerebellum revealed by trace eyelid conditioning. Learn Mem 16:86–95.

Kalmbach BE, Davis T, Ohyama T, Riusech F, Nores WL, Mauk MD. 2010. Cerebellar cortex contributions to the expression and timing of conditioned eyelid responses. J Neurophysiol 103:2039–2049.

Kelly RM, Strick PL. 2003. Cerebellar loops with motor cortex and prefrontal cortex of a nonhuman primate. J Neurosci 23:8432–8444.

Knowlton BJ, Thompson JK, Thompson RF. 1993. Projections from the auditory cortex to the pontine nuclei in the rabbit. Behav Brain Res 56:23–30.

Kosinski RJ, Neafsey EJ, Castro AJ. 1986. A comparative topographical analysis of dorsal column nuclear and cerebral cortical projections to the basilar pontine gray in rats. J Comp Neurol 244:163–173.

Kosinski RJ, Azizi SA, Mihailoff GA. 1988. Convergence of cortico- and cuneopontine projections onto components of the pontocerebellar system in the rat: an anatomical and electrophysiological study. Exp Brain Res 71:541–556.

Kronforst-Collins MA, Disterhoft JF. 1998. Lesions of the caudal area of rabbit medial prefrontal cortex impair trace eyeblink conditioning. Neurobiol Learn Mem 69:147–162.

Leergaard TB, Bjaalie JG. 2007. Topography of the complete corticopontine projection: from experiments to principal maps. Front Neurosci 1:211–223.

Leergaard TB, Lakke EA, Bjaalie JG. 2005. Topographical organization in the early postnatal corticopontine projection: a carbocyanine dye and 3-D computer reconstruction study in the rat. J Comp Neurol 361:77–94.

Legg CR, Mercier B, Glickstein M. 1989. Corticopontine projection in the rat: the distribution of labelled cortical cells after large injections of horseradish peroxidase in the pontine nuclei. J Comp Neurol 286:427–441.

Linkert M, Rueden CT, Allan C, Burel J-M, Moore W, Patterson A, Loranger B, Neves C, MacDonald D, Tarkowska A, Sticco C, Hill E, Rossner M, Eliceiri KW, Swedlow JR. 2010. Metadata matters: access to image data in the real world. J Cell Biol 189:777–782.

McBride R, Klemm W. 1968. Stereotaxic atlas of rabbit brain, based on the rapid method of photography of frozen, unstained sections. Commun Behav Biol 2:179–215.

McCormick DA, Guyer PE, Thompson RF. 1982. Superior cerebellar peduncle lesions selectively abolish the ipsilateral classically conditioned nictitating membrane/eyelid response of the rabbit. Brain Res 244:347–350.

Mihailoff GA. 1983. Intra- and interhemispheric collateral branching in the rat pontocerebellar system, a fluorescence double-label study. Neuroscience 10:141–160.

Nokia MS, Sisti HM, Choksi MR, Shors TJ. 2012. Learning to learn: theta oscillations predict new learning, which enhances related learning and neurogenesis. PLoS ONE 7:e31375.

O'Leary DD, Heffner CD, Kutka L, López-Mascaraque L, Missias A, Reinoso BS. 1991. A target-derived chemoattractant controls the development of the corticopontine projection by a novel mechanism of axon targeting. Development Suppl 2:123–130.

Paxinos G, Watson C. 2007. The rat brain in stereotaxic coordinates. London: Academic Press.

Plakke B, Freeman JH, Poremba A. 2007. Metabolic mapping of the rat cerebellum during delay and trace eyeblink conditioning. Neurobiol Learn Mem 31:105–112.

Potter RF, Rüegg DG, Wiesendanger M. 1978. Responses of neurones of the pontine nuclei to stimulation of the sensorimotor, visual and auditory cortex of rats. Brain Res Bull 3:15–19.

Powell DA, Churchwell J, Burriss L. 2005. Medial prefrontal lesions and Pavlovian eyeblink and heart rate conditioning: effects of partial reinforcement on delay and trace conditioning in rabbits (Oryctolagus cuniculus). Behav Neurosci 119:180–189.

Rüegg D, Wiesendanger M. 1975. Corticofugal effects from sensorimotor area I and somatosensory area II on neurones of the pontine nuclei in the cat. J Physiol (Lond.) 247:745–757.

Rüegg D, Séguin J, Wiesendanger M. 1977. Effects of electrical stimulation of somatosensory and motor areas of the cerebral cortex on neurones of the pontine nuclei in squirrel monkeys. Neuroscience 2:923–927.

Schindelin J, Arganda-Carreras I, Frise E, Kaynig V, Longair M, Pietzsch T, Preibisch S, Rueden C, Saalfeld S, Schmid B, Tinevez J-Y, White DJ, Hartenstein V, Eliceiri K, Tomancak P, Cardona A. 2012. Fiji: an open-source platform for biological-image analysis. Nat Methods 9:676–682.

Schmahmann JD, Pandya DN. 1997a. The cerebrocerebellar system. Int Rev Neurobiol 41:31–60.

Schmahmann JD, Pandya DN. 1997b. Anatomic organization of the basilar pontine projections from prefrontal cortices in rhesus monkey. J Neurosci 17:438–458.

Schmued L, Kyriakidis K, Heimer L. 1990. In vivo anterograde and retrograde axonal transport of the fluorescent rhodamine-dextran-amine, Fluoro-Ruby, within the CNS. Brain Res 526:127–134.

Schwarz CC, Möck MM. 2001. Spatial arrangement of cerebro-pontine terminals. J Comp Neurol 435:418–432.

Schwarz CC, Horowski AA, Möck MM, Thier PP. 2005. Organization of tectopontine terminals within the pontine nuclei of the rat and their spatial relationship to terminals from the visual and somatosensory cortex. J Comp Neurol 484:283–298.

Serapide MF, Pantó MR, Parenti R, Zappalá A, Cicirata F. 2001. Multiple zonal projections of the basilar pontine nuclei to the cerebellar cortex of the rat. J Comp Neurol 430:471–484.

Sesack SR, Deutch AY, Roth RH, Bunney BS. 1989. Topographical organization of the efferent projections of the medial prefrontal cortex in the rat: an anterograde tract-

tracing study with Phaseolus vulgaris leucoagglutinin. J Comp Neurol 290:213–242.

Siegel JJ, Kalmbach BE, Chitwood RA, Mauk MD. 2012. Persistent activity in a cortical-to-subcortical circuit: bridging the temporal gap in trace eyelid conditioning. J Neurophysiol 107:50–64.

Solomon PR, Vander Schaaf ER, Thompson RF, Weisz DJ. 1986. Hippocampus and trace conditioning of the rabbit's classically conditioned nictitating membrane response. Behav Neurosci 100:729–744.

Steinmetz JE, Lavond DG, Thompson RF. 1989. Classical conditioning in rabbits using pontine nucleus stimulation as a conditioned stimulus and inferior olive stimulation as an unconditioned stimulus. Synapse 3:225–233.

Takehara-Nishiuchi K, McNaughton BL. 2008. Spontaneous changes of neocortical code for associative memory during consolidation. Science 322:960–963.

Takehara K, Kawahara S, Kirino Y. 2003. Time-dependent reorganization of the brain components underlying memory retention in trace eyeblink conditioning. J Neurosci 23:9897–9905.

Takehara-Nishiuchi K, Nakao K, Kawahara S, Matsuki N, Kirino Y. 2006. Systems consolidation requires postlearning activation of NMDA receptors in the medial prefrontal cortex in trace eyeblink conditioning. J Neurosci 26: 5049–5058.

Terreberry R. 1987. The rat medial frontal cortex projects directly to autonomic regions of the brainstem. Brain Res Bull 19:639–649.

Thompson LT, Moyer JR, Disterhoft JF. 1996. Trace eyeblink conditioning in rabbits demonstrates heterogeneity of learning ability both between and within age groups. Neurobiol Aging 17:619–629.

Tracy JA, Thompson JK, Krupa DJ, Thompson RF. 2013. Evidence of plasticity in the pontocerebellar conditioned stimulus pathway during classical conditioning of the eyeblink response in the rabbit. Behav Neurosci 127: 676–689.

Vilensky JA, Van Hoesen GW. 1981. Corticopontine projections from the cingulate cortex in the rhesus monkey. Brain Res 205:391–395.

Weible AP, Weiss C, Disterhoft JF. 2003. Activity profiles of single neurons in caudal anterior cingulate cortex during trace eyeblink conditioning in the rabbit. J Neurophysiol 90:599–612.

Weible AP, Weiss C, Disterhoft JF. 2007. Connections of the caudal anterior cingulate cortex in rabbit: neural circuitry participating in the acquisition of trace eyeblink conditioning. Neuroscience 145:288–302.

Weiss C, Disterhoft JF. 2011. Exploring prefrontal cortical memory mechanisms with eyeblink conditioning. Behav Neurosci 125:318–326.

Weiss C, Knuttinen MG, Power JM, Patel RI, O'Connor MS, Disterhoft JF. 1999. Trace eyeblink conditioning in the freely moving rat: optimizing the conditioning parameters. Behav Neurosci 113:1100–1105.

Wells GR, Hardiman MJ, Yeo CH. 1989. Visual projections to the pontine nuclei in the rabbit: orthograde and retrograde tracing studies with WGA-HRP. J Comp Neurol 279:629–652.

Wiesendanger R, Wiesendanger M. 1982a. The corticopontine system in the rat. I. Mapping of corticopontine neurons. J Comp Neurol 208:215–226.

Wiesendanger R, Wiesendanger M. 1982b. The corticopontine system in the rat. II. The projection pattern. J Comp Neurol 208:227–238.

Wu G-Y, Yao J, Zhang L-Q, Li X, Fan Z-L, Yang Y, Sui J-F. 2012. Reevaluating the role of the medial prefrontal cortex in delay eyeblink conditioning. Neurobiol Learn Mem 97:277–288.

Wyss J, Sripanidkulchai K. 1984. The topography of the mesencephalic and pontine projections from the cingulate cortex of the rat. Brain Res 293:1–15.

Yeo CH, Hardiman MJ, Glickstein M. 1985a. Classical conditioning of the nictitating membrane response of the rabbit II: Lesions of cerebellar cortex. Exp Brain Res 60:99–113.

Yeo CH, Hardiman MJ, Glickstein M. 1985b. Classical conditioning of the nictitating membrane response of the rabbit III: Connections of cerebellar lobule HVI. Exp Brain Res 60:114–126.